

RESEARCH ARTICLE

Hailstorms in the Alpine region: Diurnal cycle, 4D-characteristics, and the nowcasting potential of lightning properties

L. Nisi¹  | A. Hering¹ | U. Germann¹  | K. Schroer¹  | H. Barras^{1,2,3,4}  | M. Kunz⁵  | O. Martius^{2,3,4} 

¹Federal Office of Climatology and Meteorology MeteoSwiss, Zürich, Switzerland

²Oeschger Centre for Climate Change Research, University of Bern, Bern, Switzerland

³University of Bern, Institute of Geography, Bern, Switzerland

⁴Mobilier Lab for Natural Risks, University of Bern, Bern, Switzerland

⁵Institute of Meteorology and Climate Research (IMK), Karlsruhe Institute of Technology (KIT), Karlsruhe, Germany

Correspondence

L. Nisi, Federal Office of Climatology and Meteorology MeteoSwiss, Locarno-Monti, Zürich, Switzerland.
Email: luca.nisi@meteoswiss.ch

Abstract

Nowcasting of hailstorms still poses a major challenge to weather services, because of the limited availability of reliable large datasets and the short spatio-temporal scales involved. Two novel Eulerian and Lagrangian hail climatologies for the Alps are applied to address important aspects of hailstorms in the Alps: the diurnal cycle, their spatio-temporal development and the lightning properties. The database contains more than 100,000 ordinary and 30,000 hail storms (2002–2017). Based on that large sample of storms, the diurnal cycle of storm initiation and evolution is studied in the context of orographic forcing and cold-front occurrence statistics. Results show that, during daytime, storms mainly initiate over the foothills (Prealps) and move towards areas with higher terrain elevations. During night-time, the storms preferably move from the foothills to the plains. Five out of 16 years of the radar-derived convective storms show a significant yearly positive hail anomaly, from which two years show relative hail-initiation maxima evenly distributed over the 24 hour without a characteristic diurnal cycle. Relative hail maxima during night-time cannot always be explained with a higher occurrence of cold fronts. Time series of storm vertically integrated liquid water content are used to separate ordinary and hail storm development. Differences are found between vertically integrated liquid and its density in cold air-mass storms. Finally, lightning data from a ground-based network are combined with the radar-derived hailstreaks and evaluated with respect to their prediction skill as a function of lead time (flash rate, density, peak current, lightning jumps). Results show that lightning data provide only modest skill-scores in nowcasting hailstorms. Only the sudden increase in lightning rate (referred to as lightning jump) may be used as additional data for hail-storm nowcasting. However, their application in automatic nowcasting systems

remains challenging as the lightning jumps occurs at various lead times in the series.

KEYWORDS

Alps, convection initiation, diurnal cycle, hail, hailstorms, hailstreak, hailswaths, lightning jump, nowcasting, VIL, VILD, weather radar

1 | INTRODUCTION

Long-term, climatological knowledge constitutes essential complementary information to weather model data in order to provide and improve precise and accurate weather forecasts and nowcasts. Climatological studies on severe convective weather events are still rare, but can reveal important information relevant to forecasting, such as their substantial contribution to total losses (e.g. Schroer and Tye, 2019). For severe convective weather and hailstorms in particular, radar data provide one of the most important and reliable sources of observational data. In the last years, growing radar archives allowed us to compile new hail climatologies in different areas of the world. Usually, single-polarization radar-based hail algorithms were employed providing gridded hail frequencies (e.g. Kunz and Puskeiler, 2010; Cintineo *et al.*, 2012; Junghänel *et al.*, 2016; Nisi *et al.*, 2016; Puskeiler *et al.*, 2016; Lukach *et al.*, 2017; Soderholm *et al.*, 2017; Warren *et al.*, 2020). At present, hail climatologies based on polarimetric measurements are not available for two reasons. First, dual-polarization radar networks in Europe have been established in most countries only recently (e.g. Saxion and Ice, 2012; Huuskonen *et al.*, 2014; Germann *et al.*, 2015). In the USA, dual-polarization algorithms have been used for several decades to study hail in storms (e.g. Balakrishnan and Zrníc, 1990; Heinselman and Ryzhkov, 2006), but at present it is still difficult to use these algorithms for hail mapping at the ground. Second, dual-polarization hail algorithms have been deployed mainly for S-band and not for C-band radars, which show significant resonance effects (Ryzhkov *et al.*, 2013). These systems, however, are installed by preference in Europe and several other regions.

The combination of single-polarization radar-based hail algorithms with thunderstorm radar tracking algorithms provides new insights into the characteristics of hailstorms. Gridded hail climatologies already provide information about the spatio-temporal distribution and occurrence frequency of hail signals. Object-based approaches such as cell tracking yield further details on individual hailstorms, such as time and location of the first signal detected by radar (hereinafter referred to as

initialization), streak characteristics such as width, length, or propagation angle, and information about the life cycle including intensification and decay stages. In the last decades, object-based approaches were successfully used for the analysis of severe convective storms (e.g. Höller *et al.*, 1994; Schmidt *et al.*, 2012; Wapler *et al.*, 2015; Tre-falt *et al.*, 2018) and for nowcasting applications (e.g. Dixon and Wiener, 1993; Johnson *et al.*, 1998; Handwerker, 2002; Roberts and Rutledge, 2003; Mecikalski and Bedka, 2006; Hering *et al.*, 2008; Zinner *et al.*, 2008; Lakshmanan and Smith, 2009; Rotach *et al.*, 2009; Nisi *et al.*, 2014). Recent studies presented solid statistical analyses based on large storm datasets created with automated tracking algorithms (e.g. Goudenhoofd and Delobbe, 2013; Wapler *et al.*, 2016; Wapler, 2017; Nisi *et al.*, 2018). These datasets allow the determination of typical storm characteristics and behaviours such as the repetitive patterns of storm initiation and precipitation that were found to be more frequent over complex terrain (e.g. Foresti *et al.*, 2018).

The simultaneous use of large datasets of convective storms by a multi-sensor methodology, e.g. radar data combined with satellite retrievals and/or lightning detections, enables us to estimate in addition the temporal evolution of various storm characteristics, which basically can be used for nowcasting purposes. In an earlier study, Nisi *et al.* (2018) reconstructed several thousands of convective storms over the Alpine area based on three-dimensional (3D) radar data and an automatic radar tracking algorithm, assuring homogeneity and objectivity over the whole dataset. In our study, we will employ an exceptional large event set consisting of more than 130,000 convective storms that were detected with the same automatic tracking algorithm (Hering *et al.*, 2008; Rotach *et al.*, 2009; Nisi *et al.*, 2014) from 4D radar measurements (x, y, z, t) between 2002 and 2017. The radar-based tracks are further combined with lightning detections and terrain height from a digital elevation model (DEM) to investigate thunderstorm and hailstorm properties and characteristics that have a potential to be used for nowcasting purposes.

The diurnal cycle of hail is strongly related to that of convective precipitation in general (Kühnlein *et al.*, 2014; Keil *et al.*, 2019). Whereas only a few studies so far have investigated the diurnal cycle of hailfall in Europe (Punge

and Kunz, 2016; Fluck, 2017), the diurnal cycle of convective precipitation has been extensively investigated for different areas of the world using rain-gauges (e.g. Wallace, 1975), satellite-based radar observations (e.g. Nesbitt and Zipser, 2003; Hirose *et al.*, 2008; Biasutti *et al.*, 2011), high-resolution ground-based radar observations (e.g. Carbone and Tuttle, 2008; Surcel *et al.*, 2010), a multi-sensor approach (e.g. Matsui *et al.*, 2010), or in combination with numerical weather prediction (NWP) modelling (Kühnlein *et al.*, 2014; Keil *et al.*, 2019). Mandapaka *et al.* (2013), who analysed the diurnal cycle of precipitation around the Swiss Alpine area using volumetric ground-based radar data, found a much stronger diurnal cycle when convective precipitation occurs (i.e. spring and summer). This is confirmed by a recent study presented by Panziera *et al.* (2018), where combined radar and rain-gauge data (Sideris *et al.*, 2014) were used to analyse sub-daily precipitation extremes over the Swiss Alps. Similar sub-daily variations are expected to be present also for hailfall.

The complex nature of orographic triggering suggests that no single index or semi-empirical rule can be directly used for nowcasting storm initiation and precipitation in general (Faulkner and Prudhomme, 1998). Previous studies found that over areas in the midlatitudes, where orographic triggering is not the main convection initiation mechanism, the diurnal cycle of storms with its typical afternoon peak is driven mainly by cold fronts as well as by air-mass convection in polar maritime air (e.g. Twardosz, 2010). The relation between hail and synoptic cold fronts was previously investigated over Switzerland by Schemm *et al.* (2016), who found that up to 45% of all radar-detected hail cells formed in pre-frontal zones. It was also found that the percentage of front-related hail initiation is highest in regions where hail is statistically less frequent – especially in northern Switzerland. This is an indication that suggests the hail maxima in the Prealps (Nisi *et al.*, 2016) to be related to orographic forcing and air-mass convection, which is probably more affected by differential heating and resulting thermal circulation as triggering mechanism.

Further parameters that could be of potential interest for nowcasting are gradients of specific storm parameters (e.g. rates of changes or jumps in radar reflectivity, water content, or lightning) prior to the occurrence of hail on the ground as well as signals that enable us to distinguish between non-severe convective cells (i.e. without hail) and hailstorms. The temporal evolution of the Vertically Integrated Liquid (hereafter VIL) and its Density (normalized using the echo top, hereafter VILD), for example, can be used to analyse 3D storm characteristics. Earlier studies (e.g. Treloar, 1996; 1998; Amburn and Wolf, 1997; Edwards and Thompson, 1998) demonstrated how VIL and VILD can be used to identify convective storms and

hail cores. VILD is particularly important during spring-time, when cold air-mass thunderstorms (including the severe ones) tend to have a low top (6–8 km in the Alps). A low top in combination with high VIL values give rise to high-intensity storms since a high amount of water content is distributed in a smaller volume. Thus, VILD enables us to better discriminate the storms. Furthermore, as with increasing VILD the hail cores tend to be deeper and more intense thus producing larger hailstones, VILD can also be used as a proxy for hail (e.g. Amburn and Wolf, 1997).

Lightning data are often used for storm verification or classification purposes (e.g. Kaltenböck *et al.*, 2009; Wapler *et al.*, 2012), for climatological analyses (e.g. Wapler, 2013; Piper and Kunz, 2017) or for nowcasting applications (e.g. Kohn *et al.*, 2011; Nisi *et al.*, 2014). The relation between microphysics and storm electrification is the subject of numerous studies (e.g. Carey and Rutledge, 1996; Dotzek *et al.*, 2001; Yair *et al.*, 2010; Yuan *et al.*, 2011; Schultz *et al.*, 2017; and many others). For nowcasting purposes, the relation between storm intensity and lightning flash rate has been investigated as well, and according to several studies, the updraught seems to be the main factor driving the lightning flash rate (e.g. Shackford, 1960; MacGorman *et al.*, 1989; Williams *et al.*, 1989; 1999; Lang and Rutledge, 2002; Goodman *et al.*, 2005; Deierling and Petersen, 2008). As suggested for example by Gatlin and Goodman (2010), a stronger updraught is associated with a higher content of water vapour, more condensation and more glaciation and therefore with an increased probability of collision among frozen hydrometeors. This leads to a stronger charge separation and higher lightning occurrence. Lightning Jumps (hereafter LJs), a sudden increase in the lightning rate, are commonly used as precursors for severe storms and hail. The drivers of LJs are found to be the fast increase of graupel mass within the thunderstorm cloud in a layer between around -10 and -40 °C in combination with enhanced updraught intensity. This parameter has been deeply investigated for some decades and is currently applied for predicting severe surface weather and cell life cycle (e.g. Williams *et al.*, 1999; Schultz *et al.*, 2009; 2011; 2015; 2017; Darden *et al.*, 2010; Gatlin and Goodman, 2010; Chronis *et al.*, 2015; Miller *et al.*, 2015; Wapler, 2017). Although not all studies are based on a large database, they have shown that LJs have a certain skill for identifying and nowcasting severe convection (e.g. Farnell *et al.*, 2017; 2018). With new and incoming satellite-based lightning imagers (e.g. Stuhlmann *et al.*, 2005; Schultz *et al.*, 2016), LJs have the potential to become a common parameter for nowcasting.

The overall objective of our study is to investigate mean characteristics and properties of convective storms including hailstorms that basically can be employed in nowcasting systems. This includes the investigation of the

spatial and temporal variability of convective storms initiation, their typical diurnal cycle, and to identify reliable precursors based on VIL, VILD and LJs that enable us to discriminate severe storms from the ordinary ones with useful lead time.

Summarizing, the aims of this study are to characterize:

1. The diurnal cycle of hail and its multi-year variability.
2. The differences in the evolution of ordinary and hail storms in space and time considering the storm vertically integrated liquid and its density.
3. The lightning properties of ordinary and hail storms, including the occurrence of LJs.

This article is organized into the following sections. Section 2 describes the investigation area and the datasets used. Because the single-polarization hail-detection algorithms as well as the tracking method are the same as used in Nisi *et al.* (2018), Section 3 provides only a brief summary of the algorithms. Section 4 presents these results of this unified study in terms of hailstorms' diurnal cycles, 4D storm characteristics using VIL-VILD during the observed storm life cycle and the storm electrical properties. Section 5 and 6 presents the discussion of these results and the conclusions, respectively.

2 | STUDY DOMAIN AND DATA

The investigation area is identical to that in Nisi *et al.* (2018) and is located in central Europe (~ 44.6 – 48.4°N and 4.8 – 10.1°E). It includes the complex orography of the central and western Alps and is currently covered by five new dual-polarization C-band Doppler radars.

2.1 | Radar observations

For this long-term study, we used three radars that are available over the entire 16-year period from 2002 to 2017, located at Albis, La Dôle and Monte Lema, in the north-eastern, western, and southern parts of Switzerland with a spatio-temporal resolution of 1 km^2 and 5 min. To avoid areas where beam-widening effects and other undesired radar issues become substantial (e.g. Nisi *et al.*, 2016), the maximum range between the location of the storms and the radar sites is limited to 160 km.

Three radar-based algorithms are used:

1. A 3D multiple-radar tracking algorithm (referred to as Thunderstorms Radar Tracking, hereafter TRT) to reconstruct entire thunderstorm tracks and to identify

initiation locations (location of the first 35 dBZ radar echo).

2. Two single-polarization radar-based hail detection algorithms, namely the Probability Of Hail (hereafter POH) and the Maximum Expected Severe Hail Size (hereafter MESHS), to identify hailstreaks.

More details on the radar data are summarized in Nisi *et al.* (2016) and presented in Joss *et al.* (1998) and in Germann *et al.* (2006; 2016; 2017).

2.2 | Digital elevation model (DEM) and NWP data

The analysis includes data from a DEM with a horizontal resolution of 25 m (Swisstopo, 2004) to identify terrain altitudes at the location of the storm as well as hailstreak initiations and maxima.

The single polarization radar-based hail detection algorithms require information on the freezing-level height (hereafter H_0). This information is extracted from analyses of the Consortium for Small-scale MOdelling (COSMO-CH; <http://cosmo-model.org/>). COSMO-CH is a non-hydrostatic, regional, high-resolution NWP model operated by MeteoSwiss. Due to model changes in the investigation period, the horizontal resolutions employed in this study are $6.6 \times 6.6\text{ km}^2$ (COSMO-7; April 2002–March 2008), $2.2 \times 2.2\text{ km}^2$ (COSMO-2; April 2008–August 2016) and $1 \times 1\text{ km}^2$ (COSMO-1, since September 2016) with a temporal resolution of 1 hr. These changes and other model modifications have no significant effects on the H_0 fields (see Nisi *et al.* (2016) for more details).

Finally, ERA-Interim reanalysis (Dee *et al.*, 2011) is used in this study to identify and compute 6-hourly frequencies of synoptic cold fronts over central Europe (Sprenger *et al.*, 2017).

2.3 | Lightning data

Lightning data provided by the Météorage – European Corporation for Lightning Detection (EUCLID, www.euclid.org) network were used for the examination of specific lightning characteristics such as LJs. An evaluation of the performance characteristics of the EUCLID lightning detections in the Alpine region is provided by Azadifar *et al.* (2016). The overall pulse detection efficiency for upward flashes was found to be 73%. For stronger pulses (peak currents higher than 5 kA) the detection efficiency for upward flashes was about 83%. The median of the absolute distance error was found to be 186 m on average.

The dataset includes positive and negative cloud-to-ground (CG) lightning as well as cloud-to-cloud (CC) and intra-cloud (IC) lightning over the Alpine area, the latter two classes combined to IC. A distinction between IC and CC lightning (inside the same convective cloud and between two distinct clouds, respectively, e.g. Uman and Krider, 1982) is not provided, but is also not relevant for this study.

The lightning dataset is available for the same 16-year study period (2002–2017) with a high spatial resolution and accuracy (median error 100–200 m according to Azadifar *et al.* (2016) and Schulz *et al.* (2016)). However, through the years, mainly in the year of 2014, the antennas and processing algorithms have been updated allowing a better detection/separation of IC lightning. Between 2002 and 2013 the average fraction of CG versus IC lightning is $70.2 \pm 13.9\%$, between 2014 and 2017 it is $26.6 \pm 9.7\%$. The predominance of IC lightning in storms have been confirmed by several authors (e.g. Price and Rind, 1993; Soriano and De Pablo, 2007). A large fraction of CG lightning indicates that the old sensors had problems prior to 2014 with the detection efficiency for IC lightning. As a consequence, all analyses that include lightning data were limited to a 4-year period (2014–2017). This time span includes a total of 36,743 ordinary storms and 5,517 hailstorms, thus is still sufficient to obtain robust results.

3 | METHODS

3.1 | Radar-derived hail proxies

POH is derived from the vertical distance between the 45 dBZ echo top height (i.e. the highest altitude at which a radar reflectivity of 45 dBZ is detected; hereafter ET45) and H0 (Waldvogel *et al.*, 1979). This quantity provides a probability estimate for hail of any size on the ground, with a scale ranging from 0% (no hail; $ET45 - H0 < 1.65$ km) to 100% (hail; $ET45 - H0 > 5.5$ km). MESHS estimates the maximum size of hailstones on the ground for diameters equal to or larger than 2 cm. It is derived from the difference between the 50 dBZ echo top height (hereafter ET50) and H0 (Treloar, 1998).

The POH and MESHS versions of Foote *et al.* (2005) and Joe *et al.* (2004), respectively, have been implemented operationally at MeteoSwiss since 2009 and are used in this study to reprocess radar data between 2002 and 2017. POH and MESHS should not be confused with other single-polarization radar-based hail detection algorithms like the Probability of Severe Hail (POSH) or the Maximum Estimated Size of Hail (MESH), both derived from the Severe Hail Index Parameter (Witt *et al.*, 1998) and commonly used, for example, in the United States.

POH and MESHS are empirical, radar-based hail detection algorithms. Since radar-based hail signals are only indirect measurements, statistical verification of the hail detection algorithms is crucial. A first verification based on independent damage reports from an automobile insurance company was presented in Nisi *et al.* (2016). Damages recorded in the 25 most populated urban areas in Switzerland were considered in the study. Despite several uncertainties related to the insurance claim reports (which result in a high FAR), POH values greater than 80% (threshold used in this study) provides POD around 90% and FAR decreases rapidly to almost 50%. More recently, Barras *et al.* (2019) presented a new verification based on several thousand of crowdsourced hail reports collected by MeteoSwiss. The verification suggests that POH and MESHS are defined too restrictively and that some hail events were missed by the algorithms. However, a positive correlation was found between the reported hail size and the radar-based size estimates (MESHS).

3.2 | Vertically integrated liquid and vertically integrated liquid density

VIL is quantified from radar columnar reflectivity, which is converted into liquid water equivalent (Greene *et al.*, 1972). In this study, VIL is obtained from three C-band Doppler radars performing volume scans at 20 elevations between -0.2° and 40° . It represents the 3D characteristics of precipitation and emphasizes convective processes in a precipitation field. Therefore, VIL is commonly used in nowcasting systems (e.g. Dixon and Wiener, 1993; Johnson *et al.*, 1998; Roberts *et al.*, 2006; Rotach *et al.*, 2009; Nisi *et al.*, 2014; Hengstebeck *et al.*, 2018). Using VIL alone for diagnosing the severity of storms can be misleading, especially in case of cold air mass and lower-top thunderstorms (e.g. Amburn and Wolf, 1997). In these cases, VILD is considered as a more homogeneous severity discriminant for different types of storms (e.g. Paxton and Shepherd, 1993). VILD is the grid-based VIL divided by the vertical extension of the storm:

$$VILD = \frac{VIL}{ET15}, \quad (1)$$

usually given in $\text{g}\cdot\text{m}^{-3}$; the 15 dBZ echo top height ET15 is used here as storm-top approximation.

To evaluate the relation between VIL and VILD we calculated Spearman's Rank Correlation coefficient at the time and location of maximum VIL (1×1 km² grid) individually and independently for each storm.

3.3 | Ordinary and hail storm detection

Operational thunderstorm nowcasting is performed at MeteoSwiss using TRT (Hering *et al.*, 2008; Rotach *et al.*, 2009; Nisi *et al.*, 2014) and the Context and Scale Oriented Thunderstorm Satellite Predictors Development (Nisi *et al.*, 2014; Hamann *et al.*, 2017). Recently, TRT has been additionally integrated into “NowPAL”, a semi-automatic operational expert system for severe storm warnings (Panziera *et al.*, 2016). The purpose of TRT is (a) to detect the position of thunderstorms, (b) to rank their severity according to thresholds of radar-based parameters (VIL, ET45, area ≥ 57 dBZ and EchoMax), and (c) to extrapolate the position for the next 60 min based on Lagrangian persistence rules. TRT is a two-step algorithm: the first part provides 2D storm-objects and related geographical and geometric information (“tracking”). The second part estimates the severity of the detected storms with a numerical value by including 3D radar data (“ranking”). Thunderstorms are classified in the four categories of weak, moderate, severe and very severe, depending on the rank value.

For this study, the TRT output from the first step is used. “Geometrical” track information is then combined with POH and MESHS data.

A number of terms like storm path, hailstreak, hailswath, storm- and hail initiation are used throughout this article (cf. section 3.4 in Nisi *et al.*, 2018). For reasons of readability, a short summary of the most important terms and definitions used in this study is provided in the list below:

- Storm path (SPA): the spatio-temporal trajectory of the storm’s centre of mass.
- Hailstreak (HST): the “hail footprints” of storms. In this study, an HST is detected when a thunderstorm contains POH values greater than or equal to 80% over an area of at least 5 km².
- Hailswath (HSW): a sequence of two or more HSTs defining an HSW. In this study, two HSTs must show a minimum time difference of 15 min to be considered independently. If a SPA has only one HST, the two are identical. According to Nisi *et al.* (2018), the large majority of hailstorms (>96%) contain only one HST.
- Storm initiation: the spatio-temporal reference of a thunderstorm detected for the first time by TRT with 35 dBZ as the minimum detection threshold of the algorithm. Thus, our storm initiation definition differs from the widely used definition of the first convective signs that occur after the formation of clouds. To minimize TRT misdetections, only storms with a minimum duration of 15 min were included in the analysis.

- Hail initiation: the spatio-temporal reference of a thunderstorm detected by TRT and showing POH values greater than or equal to 80% over an area of at least 5 km².
- Hail maximum: the spatio-temporal reference of a thunderstorm detected by TRT that shows the hailstorm maximum intensity. In this study, for storms with POH $\geq 80\%$ over an area of ≥ 5 km², a hailstorm intensity index (hereafter HII) is calculated for each 5 min time step considering POH and MESHS and their spatial extension at the time t .

$$HII_t = \sum_{i=1}^n \left(POH_i + \frac{MESHS_i \text{ [mm]}}{1 \text{ [mm]}} \right), \quad (2)$$

where n is the total number of pixels of a TRT storm cell. The HII is unitless. The time of the hail maximum along a storm path, TM , is then given by:

$$TM = \max_{1 \leq t \leq F} (HII_t), \quad (3)$$

where F is the time of storm dissipation.

Similarly to the previous study (Nisi *et al.*, 2018), storms are divided into two main classes:

1. Ordinary storms: thunderstorms with POH < 80% or an area of less than 4 km² with POH = 80% during the entire storm life cycle of ≥ 30 min (shorter-lived storms are discarded from the analyses).
2. Hailstorms: thunderstorms with an HSW of at least 5 km² with POH $\geq 80\%$ or with MESHS ≥ 2 cm and a life-cycle duration of ≥ 30 min.

3.4 | Synoptic-scale front detection

This study uses a synoptic front climatology to analyse differences in the diurnal cycle of radar-derived hailstorms. Front features are extracted from ERA-Interim reanalysis (Sprenger *et al.*, 2017). An automated detection algorithm based on the horizontal gradient of equivalent potential temperature at 850 hPa level, θ_e , is used. If the θ_e gradient exceeds $4 \text{ K} \cdot (100 \text{ km})^{-1}$, a frontal zone is detected. The thermal front parameter (TFP; Hewson, 1998) is:

$$TFP = -\nabla |\nabla \theta_e| * \frac{\nabla \theta_e}{|\nabla \theta_e|}. \quad (4)$$

A detailed description of TFP is provided by Schemm *et al.* (2016). Previous studies used this automated detection of synoptic-scale fronts in global reanalysis (Schemm *et al.*, 2015; Schemm and Sprenger, 2015) and in regional high-resolution

COSMO-7 and COSMO-2 reanalysis (Jenker *et al.*, 2010; Schemm *et al.*, 2016).

3.5 | Lightning jump detection

LJs can be computed with IC, CG or the total lightning (the sum of positive and negative CG and IC lightning; TOTLI hereafter). Schultz *et al.* (2011) demonstrated that TOTLI rather than CG temporal trends robustly correlates with severe thunderstorms. This study uses TOTLI with a temporal aggregation of 5 min to calculate LJ. Lightning is selected and aggregated over the thunderstorm area provided by TRT. In this study the “sigma” algorithm proposed by Schultz *et al.* (2011) is used for detecting LJs. It is based on the Gatlin algorithm (Gatlin, 2006; Gatlin and Goodman, 2010), which relies on the time rate of changes of the total flash rate within a thunderstorm. This article reports only the main formulae of the three-step algorithm, following Schultz *et al.* (2011; 2017). First, seven consecutive average lightning rates over a 5 min time period are computed by $f(t_0-x)$, where $x = 0, 5, 10, \dots, 30$:

$$f(t) = FR_{\text{avg}}(t) = \frac{FR(t) + FR(t-2.5)}{5}, \quad (5)$$

where $FR(t)$ denotes the 2.5 min total lightning counts of a thunderstorm and $FR_{\text{avg}}(t)$ is the resulting average lightning rate. The algorithm calculates FR_{avg} in 5 min intervals. The second step computes the six rates of change of the total flash rate $DFRDT(t_0-x)$, where $x = 0, 5, 10, \dots, 30$:

$$DFRDT_t = \frac{d}{dt}f(t) = \frac{\overline{f(t)} - \overline{f(t-5)}}{t - (t-5)}. \quad (6)$$

The third step calculates the standard deviation σ using the five most recent rates of change of the total flash rate:

$$\sigma(DFRDT_{t_0-10}, DFRDT_{t_0-15}, DFRDT_{t_0-20}, DFRDT_{t_0-25}, DFRDT_{t_0-30}), \quad (7)$$

where $DFRDT(t_0)$ is the most recent rate of change.

Finally, the sigma-level, which represents the LJ threshold value, is calculated:

$$\text{sigma level} = \frac{DFRDT_{t_0}}{\sigma(DFRDT_{t_0-10}, t_0-15, t_0-20, t_0-25, t_0-30)}. \quad (8)$$

This means that a sudden increase in lightning is considered a jump when DFRDT of the most recent time step exceeds the calculated standard deviation σ by a certain sigma-level. Each step is constantly updated with the most recent rate of change.

Several studies are based on this methodology using the 2^* (sigma-level) as LJ threshold (e.g. Schultz *et al.*, 2017; Wapler, 2017; Farnell *et al.*, 2018). Thresholds are set for the minimum lightning rate to activate the algorithm and for the sigma value. A minimum lightning rate threshold is used to avoid taking into account non-significant increments (jumps) of TOTLI. According to a sensitivity study, we set the TOTLI rate threshold to 15 flash counts in 5 min. This means that if a thunderstorm shows a smaller rate, the algorithm is not activated. With our dataset, lower thresholds increase the noise. This may not be the case with other datasets. For example Schultz *et al.* (2009) used a higher threshold corresponding to 10 flashes per minute and sigma-level = 2.

4 | RESULTS

4.1 | Diurnal cycle of storm initiation

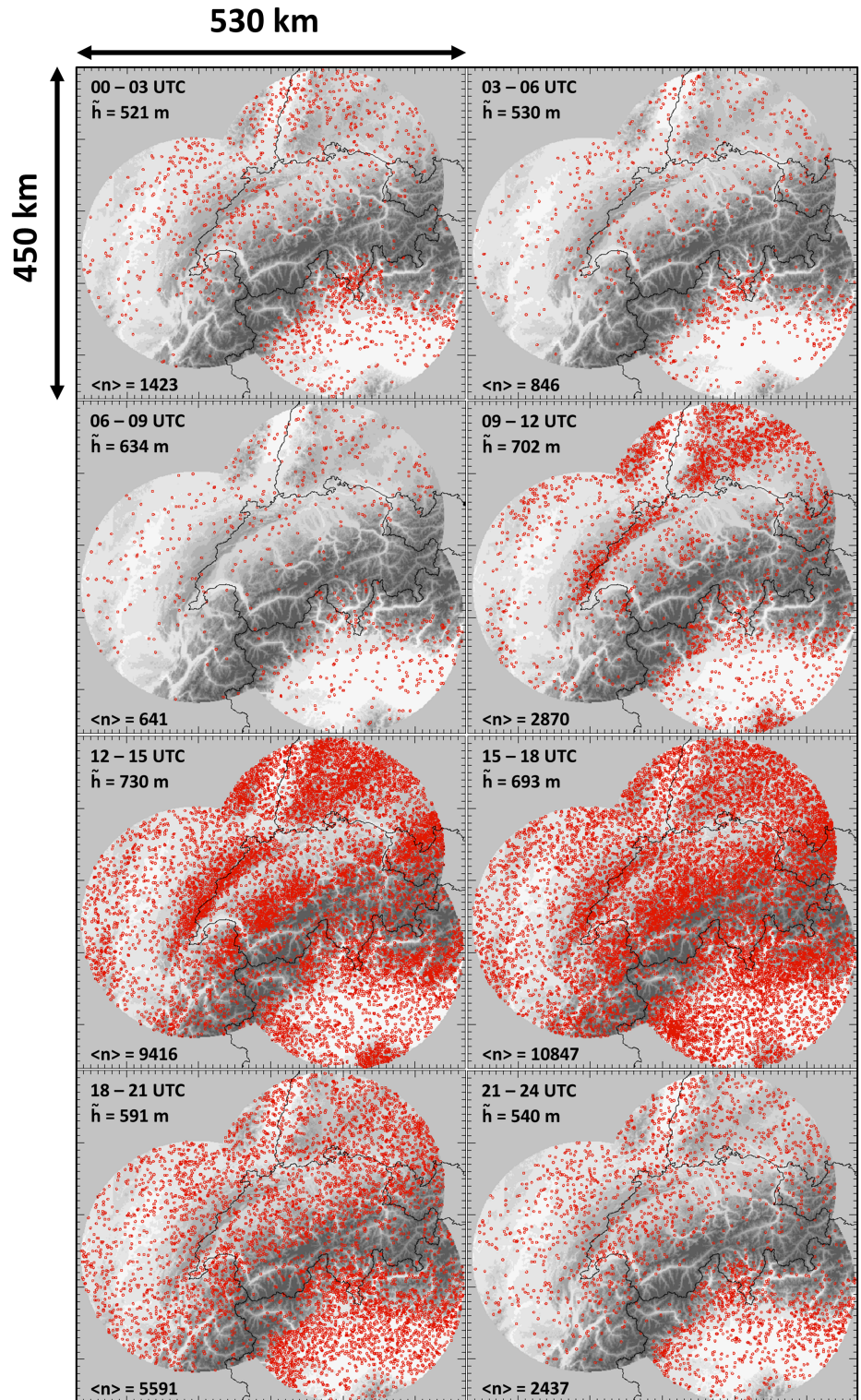
Since precipitation in the Alps is strongly modulated by the diurnal cycle, especially during the warm season (e.g. Mandapaka *et al.*, 2013), it is expected that the frequency of hailstorm initiation also shows a distinct diurnal distribution.

Results show that both the frequency and the preferred locations of hailstorm initiation (POH >80%) are strongly controlled by the time of the day. Most of the events occur after noon and last until the early evening hours (Figure 1). Over the Alpine main ridge, storm initiations are rare at any time. North of the Alps the initiation locations are almost homogeneously distributed with a very low frequency between night-time and the mid-morning hours (0000–0900 UTC). South of the Alps the spatial distribution is more heterogeneous with several clusters present along the southern foothills.

Between 0900 and 1500 UTC clusters of initiation locations occur along the Jura Mountains and over the hilly terrain in southern Germany and western France. In the afternoon and early evening hours (1500–2100 UTC), initiation locations are preferably found at higher altitudes on both sides of the Alps: initiation hotspots during that time frame are mainly located over the rough terrain along the southern and northern slopes of the Alpine chain. During late evening (2100–2400 UTC), a storm initiation cluster remains along the southern foothills comparable to the situation at 0000–0300 UTC, whereas the pattern elsewhere becomes again more homogeneous.

To statistically relate hailstorm initiation location and terrain height, we calculated for all 3 hr time slices displayed in Figure 1 median altitudes of storm initiation locations. The lowest height (521 m) is found between 0000 and 0300 UTC, the highest between 1200 and 1500

FIGURE 1 Hailstorm initiation locations (red circles) by 3-hourly intervals. \tilde{h} is the average terrain altitude at storm initiation locations; $\langle n \rangle$ is the number of individual storms considered. Local time = UTC + 2 hr



UTC (730 m). The results show that at night hailstorms tend to initiate over lower altitude mainly close to the foothills, whereas during daytime, especially in the afternoon, storms tend to initiate over higher altitudes, which correspond to areas with a rough terrain. The distribution of the altitudes of hailstorm initiation location is presented in Figure A1 (Appendix A).

This relation is further examined by the diurnal distributions of the median storm initiation location altitudes \tilde{h} and the respective interquartile range 25–75% shown in Figure 2. Two locations along each storm trajectory are considered in this analysis: the location of storm initiation (recall: radar echo reaching 35 dBZ) and the location of the hail maxima according to the combination POH / MESHs

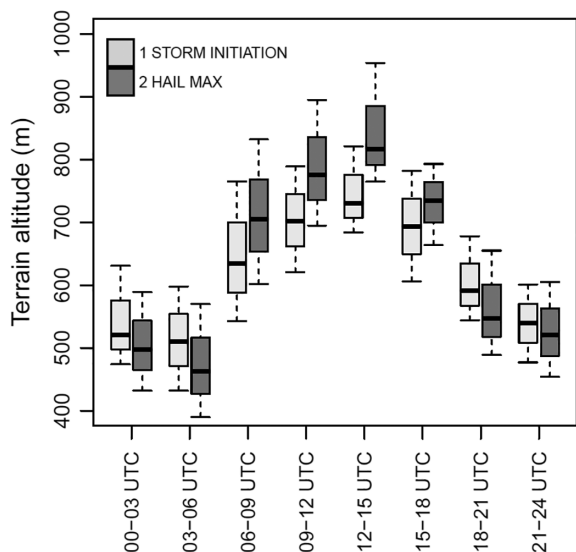


FIGURE 2 Diurnal cycle of the terrain altitude (median) of two positions along storm trajectories: (1) location of storm initiation (hailstorm only, light grey boxes) and (2) location of maximum hail intensity (dark grey boxes). The bottom and top of the black bar show the 25th and 75th percentiles

(cf. Section 3.3). For both locations, the median value is lower in the evening and in the night and higher in the afternoon. During night-time, the median altitude of initiation locations is higher compared to the median altitude of hail maxima. The spread of the interquartile range is slightly larger during daytime.

In the next step, we investigate the annual variability of the radar-detected hailstorms motivated by the fact that convective activity or predisposition has been shown to have a very large annual and multi-annual variability across Europe, partly related to large-scale flow conditions teleconnection patterns, or sea-surface temperature (e.g. Mohr *et al.*, 2015; Rädler *et al.*, 2018; Piper *et al.*, 2019). The hypothesis here is that when large-scale mechanisms become more dominant in certain years and in others not, also the daily cycle of convective activity or hailstorm frequency, respectively, should be affected. The overall hailstorm frequency (Nisi *et al.*, 2018) was used to calculate the annual variability of the diurnal cycle of hailfall. Between 2002 and 2017, five years show positive hail anomalies, namely the years of 2003, 2006, 2008–2009, and 2017 (Figure 3). Surprisingly, the year of 2003 with the highest hailstorm frequency in Switzerland is that of the most severe European heatwave associated with a persistent long-wave Rossby pattern (so-called omega-pattern), which usually suppresses convective activity as observed in several European countries (e.g. Mohr *et al.*, 2015). Even in Switzerland the overall number of storms in 2003 was lower compared to the average frequency. However, a higher percentage of

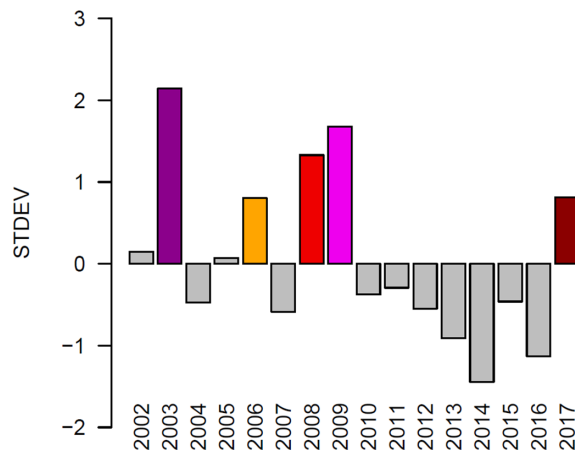


FIGURE 3 Hail (POH > 80%) annual hail anomalies. To capture the year-to-year variability, standardized annual anomalies (Wilks, 2006; Nisi *et al.*, 2016) are calculated. Years showing a positive hail anomaly (> +0.5 standard deviations) are highlighted with colours

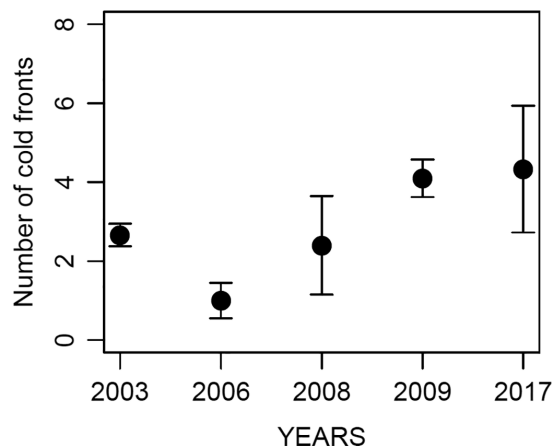


FIGURE 4 Seasonal average and standard deviation of cold-front frequency. Five warm seasons (April–September) with positive hail anomaly are considered. The domain is 44–48°N, 5–11°E, including the entire radar domain used in this study. Spatial resolution is 1°

severe hailstorms (~40%) was observed compared to the 15-year mean (~17%: Nisi *et al.*, 2018). The other years show hail frequencies around the mean or with negative anomalies.

Thermo-topographical flow together with synoptic forcing (e.g. Schemm *et al.*, 2016) are the main triggering mechanism of convection in the Alps. Therefore, the cold-front frequency of years showing a positive hail anomaly is analysed (Figure 4) and the location of hailstorm initiation is investigated with a DEM. In general, it is expected that years which show a non-typical diurnal cycle (without afternoon maximum) show a higher frequency of cold fronts.

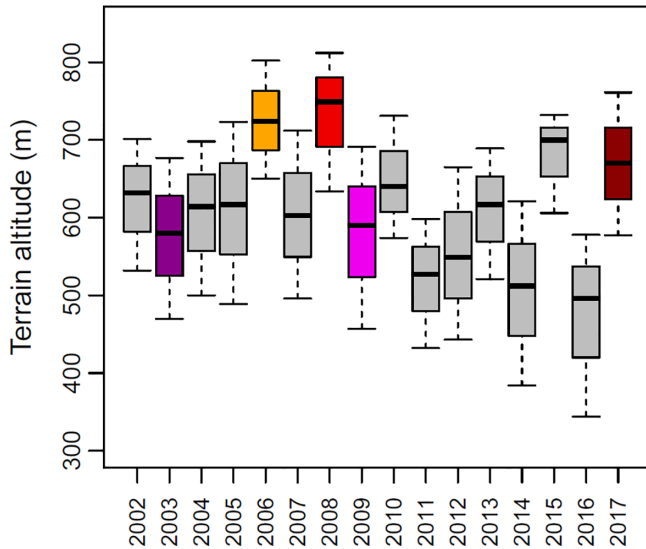


FIGURE 5 Yearly distribution of the median terrain altitude of locations of hailstorm initiations (cf. Figure 1). Coloured bars show years with positive hail anomaly (same colours as Figure 3). The bottom and top of the black bar show the 25th and 75th percentiles

The annual distribution of the mean terrain altitude of locations affected by hail initiations is presented in Figure 5. The hail-rich years are highlighted with colours. The years 2006, 2008 and 2017 show higher median altitude values than the also hail-rich years 2003 and 2009. These higher median altitudes are paralleled by a pronounced diurnal cycle as can be seen in the standardized hailstorm initiation anomalies in Figure 6. Here the years of 2006, 2008 and 2017 show strong positive anomalies during afternoon hours only. The diurnal cycles of 2006 and 2008 are almost similar. The diurnal cycle of 2003 is contrary to that of 2009: the former show two relative maxima, one in the night and one in the afternoon. The year 2009 shows a small increase in the frequency around midday.

4.2 | Vertically integrated liquid

The frequency distributions of VIL and VILD values for ordinary and hail storms differ significantly (Figure 7). Ordinary storms with moderate or high VIL values ($>10 \text{ kg}\cdot\text{m}^{-2}$) and hailstorms with low VIL values are relatively rare. Ordinary storms show a low median VIL and VILD of about $3 \text{ kg}\cdot\text{m}^{-2}$ and $0.2 \text{ g}\cdot\text{m}^{-3}$, respectively. Hailstorms show a more Gaussian frequency distribution with high standard deviations (STDEVs): median VIL and VILD values of about $19 \text{ kg}\cdot\text{m}^{-2}$ (25th percentile: $13 \text{ kg}\cdot\text{m}^{-2}$; 75th percentile: $26 \text{ kg}\cdot\text{m}^{-2}$) and $0.9 \text{ g}\cdot\text{m}^{-3}$ (25th percentile: $0.6 \text{ g}\cdot\text{m}^{-3}$; 75th percentile: $1.2 \text{ g}\cdot\text{m}^{-3}$), respectively.

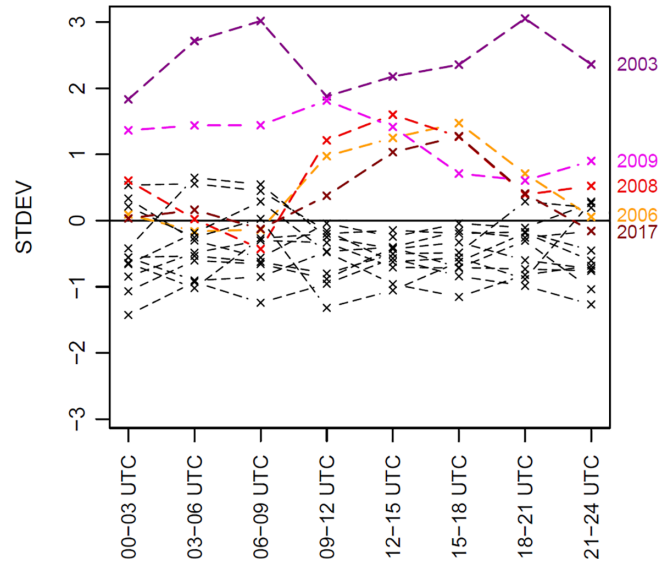


FIGURE 6 Diurnal pattern of the number of hail initiation locations (standardized anomaly) by year. Each anomaly is calculated independently for the respective time interval of 3 hr. Years showing a global seasonal positive hail anomaly are highlighted with colours (same colours as in Figure 3). To capture the 3-hourly variability, standardized anomalies (Wilks, 2006; Nisi *et al.*, 2016) are calculated

The VIL-VILD Spearman's Rank Correlation coefficients are calculated using a database of 102,927 ordinary storms and 31,823 hailstorms (Table 1). The overall correlation scores between 2002 and 2017 are 0.69 (significance level 0.05, $t = 169$, $p = 2.2 \cdot 10^{-16}$) for ordinary storms and 0.77 (significance level of 0.05, $t = 577$, $p = 2.2 \cdot 10^{-16}$) for hailstorms. Overall, correlation scores are higher for hail- than for ordinary storms. Lowest correlations are found in low-topped cold air-mass storms, which are usually classified as "ordinary" storms. A seasonal cycle is found in the correlation scores with minimum in April (0.64 ordinary storms and 0.68 hailstorms) and maximum in July (0.81 and 0.89, respectively).

VIL-VILD time series have been calculated for testing their potential as nowcasting precursor of hail (VIL time series are presented in Figure 8; VILD time series show no significant differences and therefore are not presented in this article). For this purpose, storm cells with different life-cycle durations have been investigated. For ordinary storms, VIL values are substantially lower compared to hailstorms. They also peak at the time of EchoMax or 5 to 10 min earlier or later, respectively. For hailstorms, VIL peaks at the time of both hail initiation and maximum hail-fall (cf. Section 3.3), for the former with a slight delay of 5 min. Further, whereas VIL after reaching the hail maximum drops to values prior to that point, that is, having the form of a Gaussian distribution, it remains for the location of hail initiation over a longer period of time at higher

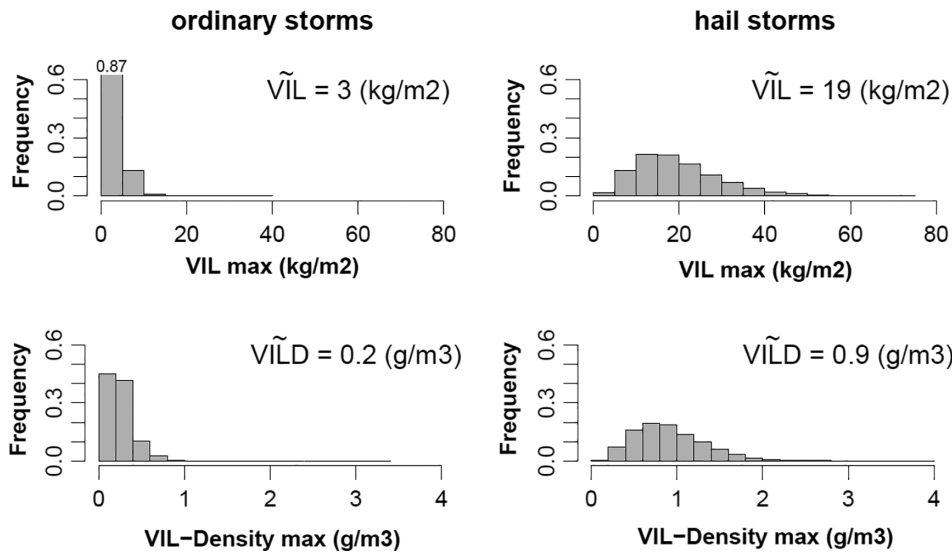


FIGURE 7 VIL and VILD frequency distribution for ordinary and hail storms. Histograms refers to individual storms. \tilde{VIL} and \tilde{VILD} are the median and the number above the highest bar of the histogram corresponds to its frequency

values. In addition, the interquartile range also increases at this point, which is not the case when considering the hail maximum.

4.3 | Hailstorm lightning properties

To assess the skill of lightning characteristics such as LJ to be used as a predictor for hail, we restrict the analyses to the years between 2014 and 2017, for which the EUCLID lightning network reliably registered IC in addition to CG flashes. During that period, the applied radar algorithms detected 36,743 ordinary and 5,517 hailstorms with different life-cycle durations (Figure 9).

Overall, for both storm types, IC flashes dominate both CG- and CG+, thus the histograms of TOTLI are similar to that of IC strokes. In addition, median values confirm that CG+ are relatively rare for both storm categories. The frequency distributions of CG- and IC are similar for both ordinary and hail storms, whereas the distribution of CG+ is significantly skewed to the right. Hailstorms show both a higher number of lightning flashes (Figure 10) and higher peak currents (Figure 13) compared to ordinary storms. The median of the number of all flash types for ordinary storms is low (≤ 6), but with a maximum value of more than 100 flashes per storm. By contrast, hailstorms show higher median number of flashes: 39 (CG-), 6 (CG+) and 127 (IC). For this storm class, single storm maximum values are significantly higher: 2953 (CG-), 752 (CG+) and 18019 (IC). Considering median values, the difference between hail- and ordinary storms is very high for CG- (+1300%) and IC (+2116%), but less significant for CG+ (+300%).

The fraction of flash types, taking into account each time step of the entire storm’s life cycle, remains almost

TABLE 1 Storm-based VIL-VILD correlation at the moment of maximum VIL

Period	Ordinary storms (>30 min) Spearman’s rank correlation coefficient (No. of storms)	Hailstorms (POH >80%) Spearman’s rank correlation coefficient (No. of storms)
April	0.64 (5,667)	0.68 (684)
May	0.72 (13,920)	0.78 (3,692)
June	0.74 (21,799)	0.84 (9,323)
July	0.81 (25,363)	0.89 (10,491)
August	0.69 (23,621)	0.78 (5,988)
September	0.56 (12,557)	0.67 (1,645)
Apr–Sep	0.69 (102,927)	0.77 (31,823)

constant for both storm categories (not shown). The fraction of IC is between 60 and 79%, of CG- between 12 and 38% and of CG+ between 2 and 11%. The large predominance of IC is present throughout the entire storms’ life cycles. No substantial difference is visible when comparing ordinary with hail storms. Furthermore, no substantial difference in the lightning type fraction is visible at the moment of EchoMax, hail initiation and hail maximum for the different storm groups.

In the next step, we investigate whether the time series of lightning frequency, lightning density and peak current show any systematic differences among the storm types related to EchoMax, hail initiation, and hail maximum (cf. Section 3.3).

The distinction between ordinary and hail storms is evident if comparing time series of flash rates and densities (Figures 11 and 12). Increases of lightning rates and

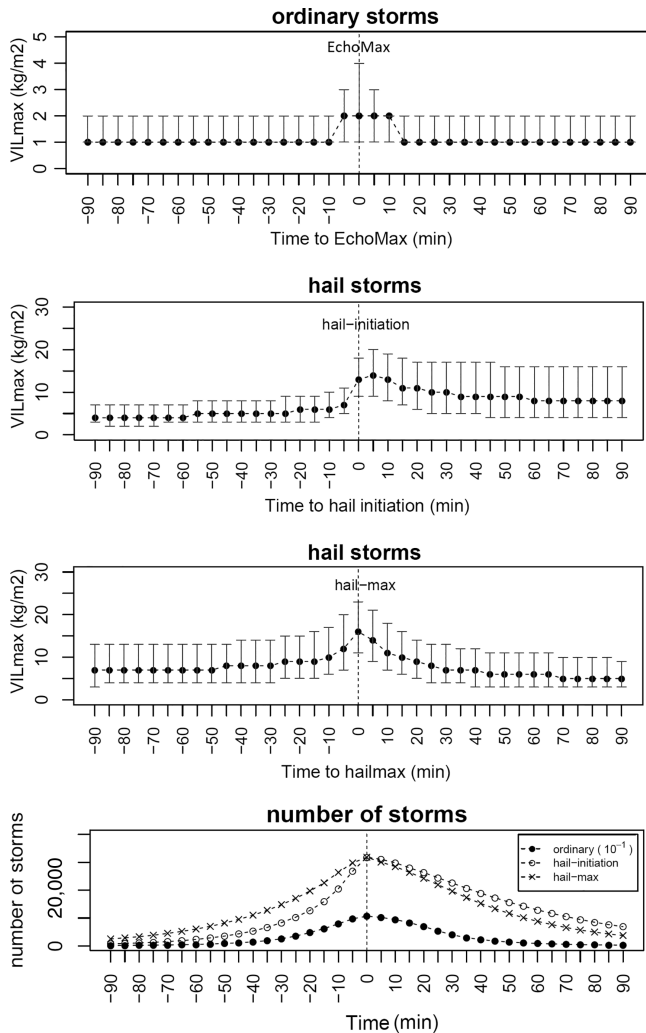


FIGURE 8 VIL time series for ordinary and hail storms. Reference time ($t = 0$) refers to the moment of EchoMax for ordinary storms and for hail initiation and hail maximum for hailstorms, respectively

densities are present 10 min before hail initiations. These increases are visible for IC, CG- and TOTLI rates and densities. IC and TOTLI time series are very similar because IC represents the large majority of flash types at all lead times. CG+ is a relatively rare flash type and values are close to 0.

Overall, the peak current of ordinary storms is weaker than that of hailstorms (Figure 13). For ordinary storms median values are close to 0 for all lead times, 75th percentiles are around 1 kA for CG+ and 1–2.5 kA for CG- (Figure 13). An increase in the peak current of CG- is found at the time of EchoMax (time = 0). A more evident signal of change over time is visible in the peak current time series of hailstorms. Median values of CG+ peak currents show an increase starting 15 min before hail initiation. The increase of CG- peak currents starts earlier (40 min before hail initiation) and becomes abrupt in close proximity to hail initiations. For both CG+ and CG- maximum peak

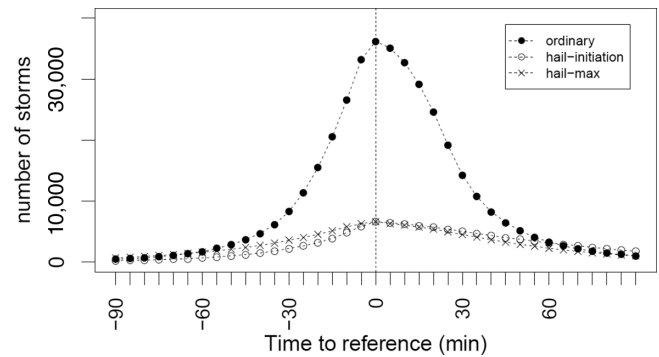


FIGURE 9 Number of storms for different lead times considered in the lightning analysis. Reference time $t = 0$ corresponds to MaxEcho, hail initiation or hail maximum. Similar to Figure 8, but here only storms between 2014 and 2017 are considered

currents are reached 10–15 min after hail maximum, with median values ranging from 7 to 11 kA. In later stages of hailstorm life cycles, lightning peak currents decrease slowly.

As we have seen in the previous analyses, there are some robust signals in the lightning data either prior to Or directly at the time of maximum radar echo in case of ordinary storms, or at the time of hail initiation and hail maximum estimated from the radar. This leads to the next question: whether LJ used by some authors as hail proxy also provides robust signals, that is, signals that can be assigned uniquely to the highest radar intensities. Time series of LJs occurrence for different sigma-level magnitudes (cf. Section 3.5) are shown in Figure 14. Overall, the following statements can be inferred from the time series. First, weaker LJs (i.e. LJs with a lower sigma-level) are more frequent. Second, the stronger the storms are (i.e. larger MESH values), the more frequent are the LJs. Third, ordinary storms show a very low relative frequency of LJs throughout their life cycle. These frequencies (0–0.05) are low and constant for all lead times. Only sigma-level magnitudes of 1.0 show a slight frequency increase for lead times between –50 and –20 min. Hailstorms by contrast have a relative LJs frequency maximum with weak sigma-level magnitude (1.0) around 20 min prior to hail initiation. For higher sigma-level magnitudes, LJ frequencies are more constant and the occurrence is shifted more and more after the time and location of hail initiation.

Isolated discontinuities and maximum values in the time series must be interpreted with care as they are a statistical consequence of the reduced sample size and increased uncertainty. For example, hailstorms with $MESH \geq 6$ cm show an isolated maximum with relative frequency of about 0.3 for a lead time of –60 min (1 hr before hail initiation). Storms producing severe hail sizes

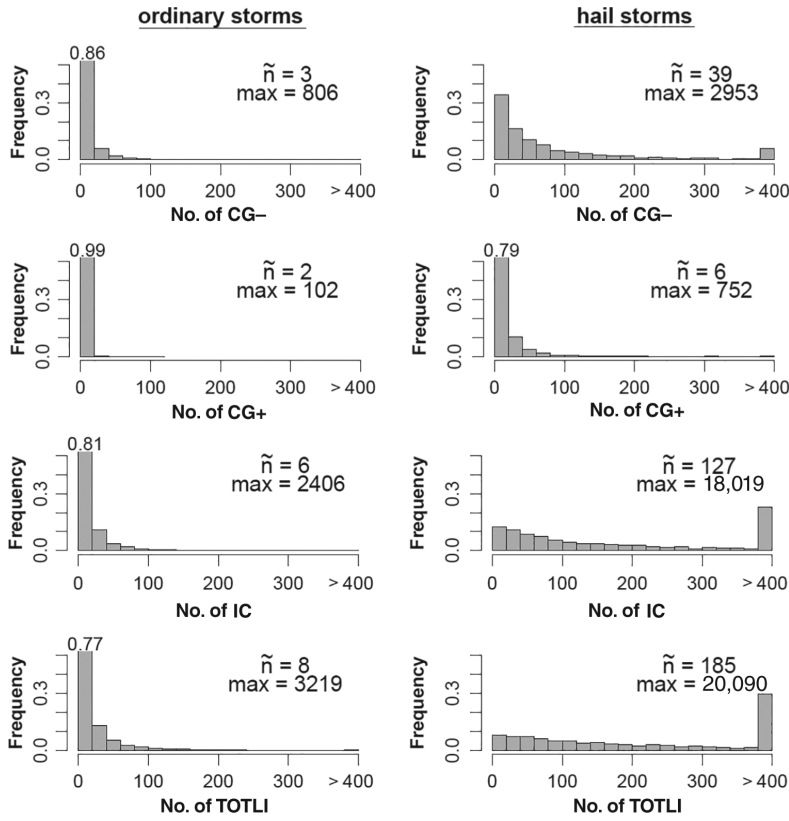


FIGURE 10 Frequency histogram for different flash types (CG-, CG+, IC; all peak currents) for both ordinary and hail storms. The distribution of TOTLI is also provided. Histograms refers to individual storms. \tilde{n} is the median, max is the maximum number of lightning flashes in a storm and the number above the highest bar of the histogram corresponds to its frequency

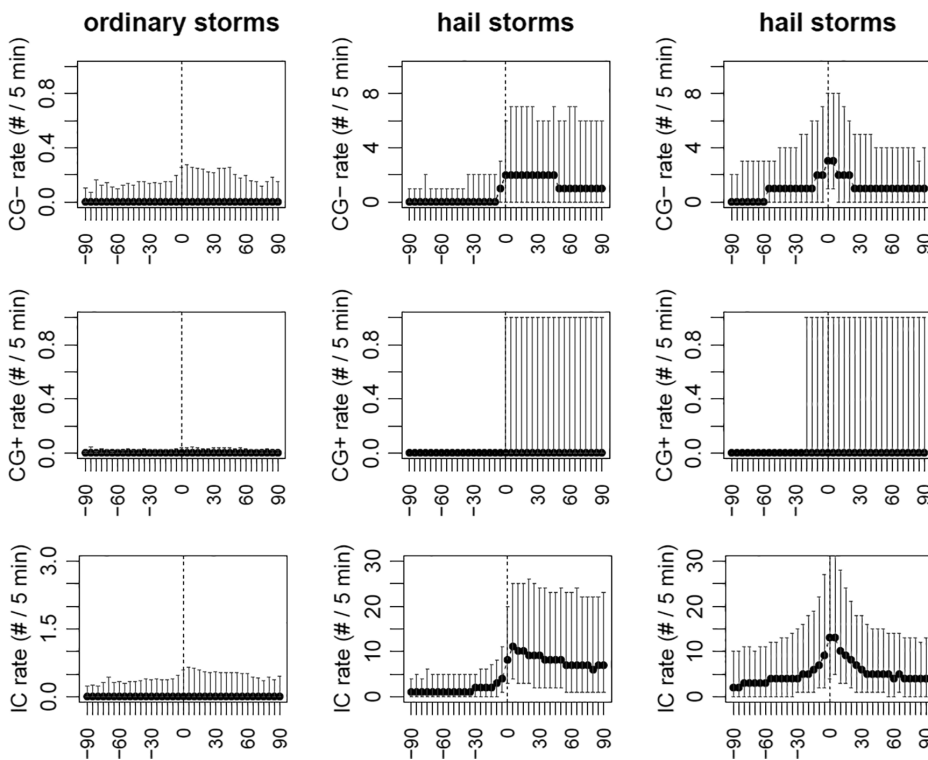


FIGURE 11 Lightning rate time series (median, 25th and 75th percentile) for ordinary and hail storms. IC, CG+ and CG- rates are calculated separately. TOTLI is substantially dominated by IC and therefore is not visualized. Reference time ($t = 0$) refers to the moment of EchoMax for ordinary storms (left column) and for hail initiation (centre column) and hail maximum for hail storms (right column), respectively. ‘#’ here means ‘number’

are quite rare and, as reported in Nisi *et al.* (2018), they tend to be explosive at early stages, reducing drastically the time span between storm initiation and hail initiation (e.g. Kunz *et al.*, 2018). For these reasons, only seven

storms that have produced very large hailstones (≥ 6 cm) in their lifetime already existed 60 min before hail initiation, and those storms increase the normalized frequency in the time series dramatically.

FIGURE 12 Same as Figure 11, but for lightning density

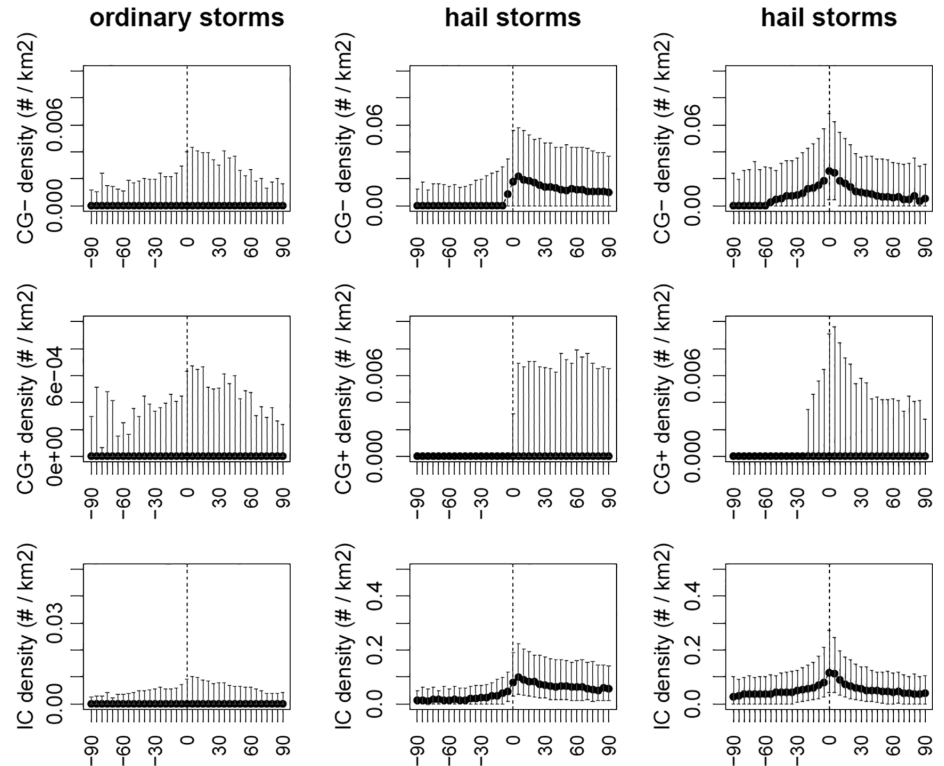
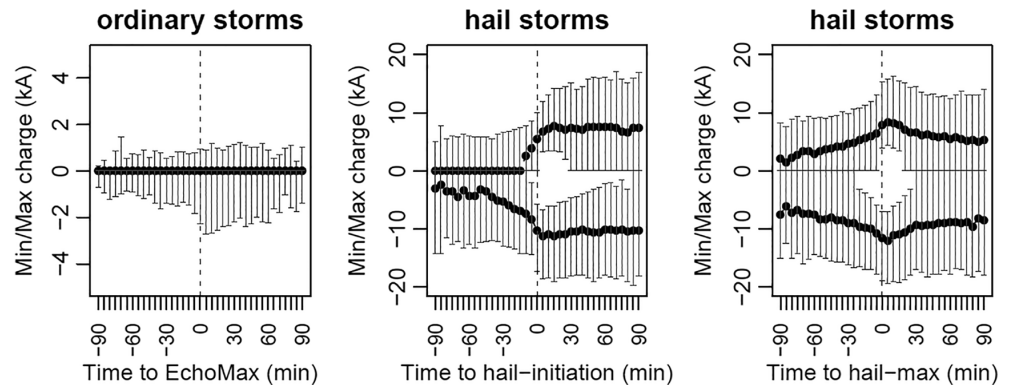


FIGURE 13 CG lightning peak current time series for ordinary and hail storms. The distribution (median, the 25th and 75th percentiles) of negative or positive peak currents are shown. Reference time ($t = 0$) refers to the moment of EchoMax for ordinary storms (left) and for hail initiation (centre) and hail maximum (right) for hailstorms, respectively



With the aim of investigating the potential of LJs as precursor of hail, the relative occurrence of LJs are investigated and shown in Figure 15. The weakest LJs (sigma-level magnitude 1.0) were considered in this analysis. The histogram (a) shows LJ occurrence before EchoMax for ordinary storms and before hail initiation for hailstorms. The very small relative frequency reveals that ordinary storms only rarely produce LJs before EchoMax, which is also in line with the perception that LJs are due to large graupel masses. Hailstorms, on the other hand, may produce a single LJ before hail initiation with a frequency of about 0.43–0.47, depending of the storm's intensity. Multiple LJs (two or more) are less frequent with relative frequencies between 0.2 and 0.25. These relative frequencies remain almost constant for all hailstorm types.

Considering entire storm life cycles (Figure 15b), ordinary storms do not show substantial differences as already discussed above. Only a small minority of storms produce one or more LJs. However, hailstorms show a different behaviour of the frequencies: by increasing the hailstorm intensity, frequencies of single LJs increase from 0.49 to 0.77, and frequencies of multiple LJs from 0.33 to 0.61.

Table 2 summarizes different skill scores computed from the contingency table of categorical verification (Wilks, 2006) using LJs (sigma-level magnitude 1.0) for nowcasting hailstorms and for discriminating hail from ordinary storms (see Table B1 in Appendix B). In the first case, only the storm life cycle before hail initiation is considered. A POD of about 0.45 and an FAR of about 0.3 are obtained for a median lead time of 20 min. In the second case, the entire storm life cycle is considered. LJs perform

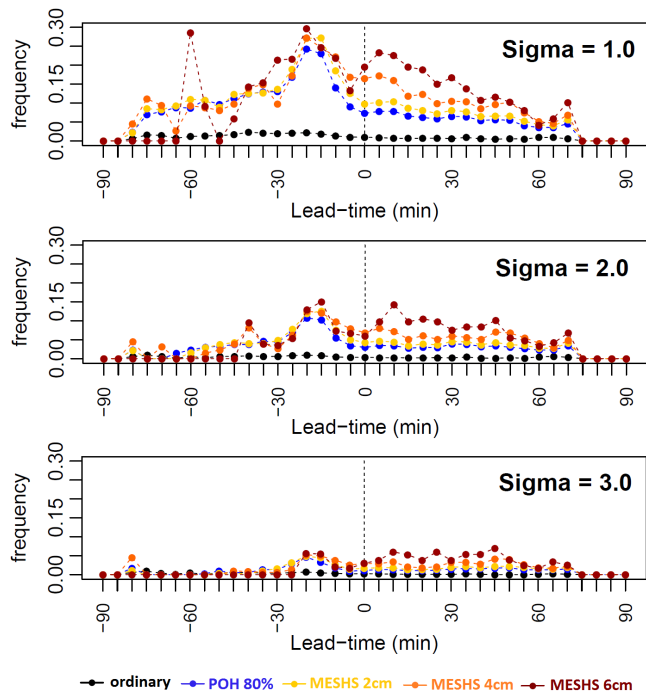


FIGURE 14 LJs normalized frequency time series for ordinary and hail storms. According to Schultz *et al.* (2009), TOTLI has been used to calculate the jumps. Three LJ sigma-level magnitudes 1.0, 2.0 and 3.0 are shown. Reference time t_0 is EchoMax for ordinary storms and hail initiation for hailstorms

slightly better in discriminating hail from ordinary storms rather than nowcasting hail initiation. Despite the comparatively low values of the skill score, these first results show some potential for real-time nowcasting applications.

5 | DISCUSSION

The results presented in Section 4.1 show that during daytime the median altitude of locations where storm initiation occurs is lower than the median altitude of locations where the first hail signal is recorded. Therefore, storms predominantly move upslope during intensification and mature stages, from the plain to the foothills and to the higher mountain chains (e.g. Prealps toward the Alps). During night-time, on the contrary, storms tend to initiate over areas with a slightly higher terrain altitude as compared to where they produce hail, suggesting a propagation from the foothills to the plains. The Alpine pumping, a larger-scale thermal circulation caused by differential

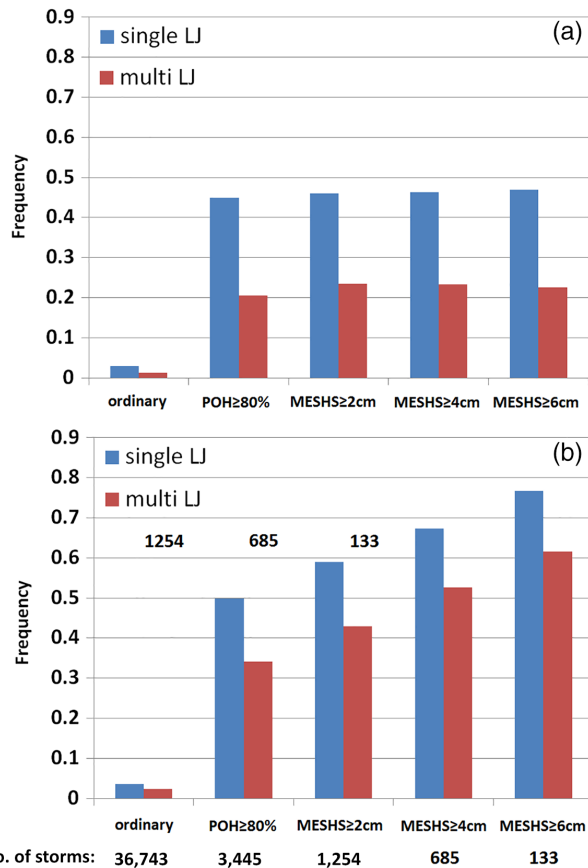


FIGURE 15 Relative frequency of LJs for ordinary and hail storms. The lowest sigma-level magnitude used in this study (1.0) is taken. Different hailstorm intensities are considered (POH >80%, MESHS >2, 4 or 6 cm). Panel (a) only considers LJs before hail initiation, (b) considers the entire storm life cycle (i.e. the lead time could be negative compared to the hail initialization). Blue bars indicate single LJs, red bars multiple events with two or more LJs

heating (Bica *et al.*, 2007), may play a major role in this pattern.

Especially in the warm season, Alpine pumping leads to a horizontal transport of air from the plains to the Alps during daytime and vice versa during night-time (e.g. Weissmann *et al.*, 2005; Bica *et al.*, 2007). Alpine pumping can produce local convergences and thermal fronts (e.g. Schemm *et al.*, 2016) as well as enhance vertical wind shear (e.g. Trefalt *et al.*, 2018) and orographic lifting (e.g. Lugauer and Winkler, 2005). All these elements can promote convection initiation and sustain the storm intensification. During daytime, the horizontal transport of air towards the mountains (valley winds and upslope wind system) results

Storm phase:	POD	FAR	CSI	Bias	HSS
Before hail initiation only	0.45	0.30	0.38	0.65	0.50
Entire life cycle	0.55	0.30	0.44	0.78	0.56

TABLE 2 Probability of detection, false alarm rate, critical success index and bias of LJ (sigma-level 1.0) as a predictor for hailstorms with an average lead time of 20 min

in horizontal flow convergences at low levels and resulting uplifts assuming incompressibility. This mechanism may be considered as major trigger for convection. During night-time, the inverse mode of Alpine pumping produces thermal fronts and convergences due to katabatic wind systems. These effects may be in addition enforced by the outflow of earlier storms in the mountains. It can thus be speculated that the Alpine pumping drives the movement of the storms especially in the case of air-mass convection at their initiation and intensification stages. Alpine pumping and daily subsidence over the plains may also be the reason for later convection initiation over the plains (e.g. in the Po Valley, figure 10 in Nisi *et al.*, 2016). However, the patterns of hailstorm occurrence under Alpine pumping conditions and in particular, how these patterns are modulated by large-scale flow over the study domain needs further investigation.

Years with a strong positive anomaly in the number of hailstorms show different distributions of hail occurrence during the day. The years of 2006, 2008 and 2017 show an intensified diurnal cycle of hail as compared to the multi-year average with a distinct maximum in the late afternoon hours. Furthermore, hailstorms initiated at higher terrain altitudes, where orographic triggering may be stronger. The years of 2003 and 2009 do not show such a distinct diurnal cycle in hailstorm anomaly, and storms initiated preferably at lower terrain altitude. The main storm trigger in years with a pronounced diurnal cycle in the hail anomaly most likely is related to thermo-topographic forcing. In the Alps, roughly half of hailstorms are produced by air-mass instability, while approximately 45% of all storms have been associated with frontal forcing (Schemm *et al.*, 2016). The years 2006 and 2008 show a lower than average cold-front frequency as compared to the other hail-intensive years (Figure 4). The pronounced diurnal cycle with maximum hail occurrence in the afternoon suggests that in these years the fraction of air-mass storms without a front as trigger was higher. Hail occurrences in 2003 and 2009 show relative maxima even during night-time (Figure 6). The maxima in 2009 can be at least partly explained by a slightly higher average cold-front frequency (68% of hailstorms triggered by synoptic forcing). The features in 2003, a summer with unusually hot weather conditions over Europe, are characterized by a lower number of ordinary thunderstorms but a high fraction of hailstorms (Nisi *et al.*, 2018). Despite the relatively low cold-front occurrences, the very high potential instability may explain the relative maximum during night-time in 2003. The year 2017 shows a pronounced diurnal cycle and a higher cold-front frequency which is comparable with 2009. For these reasons, the frequency of synoptic forcing alone (i.e. low-level moisture advection and capping inversion

reduction through upper-level cold air advection) can only marginally explain the differences in hail occurrence behaviours for different years. Preconditioning environments, including the availability of low-level moisture, steeper lapse-rates and high wind-shear conditions are predominant factors for the occurrence of severe convection (e.g. Brooks, 2009) and should be considered in future studies.

Hailstorms show VIL and VILD values that are significantly higher than the ordinary, non-hail-producing storms. To support the formation of hail cores, the storms must satisfy some ambient conditions like high wind shear and strong and persistent updraughts (e.g. Foote, 1984; Lombardo and Colle, 2011). Strong updraughts ingest large amounts of humidity into the storms, thereby increasing VIL. Distributions of VIL and VILD are similar, indicating that the two parameters are not independent. The correlation between VIL and VILD is higher for hailstorms than for ordinary storms. Considering median values, the difference between the two storm types is higher for VIL (633%), than for VILD (450%). VILD considers the vertical extent of the storm: large amounts of water content in hailstorms are compensated by a greater vertical extent, which reduces the density. The utilization of VIL or VILD for hail diagnosis and nowcasting has been proposed by several authors (e.g. Amburn and Wolf, 1997; Billet *et al.*, 1997). However, the correlation between VILD and hail and severe storms was also debated (Edwards and Thompson, 1998; Maddox *et al.*, 1999). According to Edwards and Thompson (1998), the added value of VILD compared to VIL for inferring the presence of severe hail is limited. Correlation scores between storm-based VIL and VILD show a seasonal cycle. Higher VIL-VILD correlation scores for both ordinary- and hailstorms are found in July. Larger differences are found especially in cold air mass, low-topped storms. In these cases VILD provides a robust proxy for the severity of storms and can be used to better discriminate hail-bearing storms. However, these two parameters cannot be used as hailfall precursors. Time series show strong gradients (i.e. rapid increase in VIL or VILD) only shortly before hail initiation, and usually VIL_{max} and $VILD_{max}$ are reached only at the time of maximum hail intensity. For t reasons, the two parameters may be used to diagnose the initiation of hailfall, but not as precursors in the nowcasting algorithms. Despite being challenging, a VIL or VILD forecast (e.g. Nisi *et al.*, 2014) would be more promising for nowcasting applications.

Lightning characteristics and properties are radar-independent parameters and often used as precursors for severe convection (e.g. Knapp, 1994; Williams *et al.*, 1999; Kohn *et al.*, 2011; Schultz *et al.*, 2011). Overall, ordinary storms show a weaker electrical activity

compared to hailstorms. The difference is evident for CG- and IC, but not for CG+, which occur significantly less frequently. According to Lang and Rutledge (2002), the updraught volume and related greater amounts of liquid and solid precipitation was the only significant difference found between CG+ producing and non-producing storms. Since ordinary storms selected in this study may produce large amounts of rain without hail, it is possible that in this case the occurrence of CG+ cannot be a discriminant for separating correctly hail storms from the ordinary ones. Even the ratios between the flash types remain almost constant over a long period of time and show no significant changes at the time of EchoMax, hail initiation or hail maximum.

Spatial and temporal flash occurrences, represented by flash density and rate, show an increase on approaching the moment of hail initiation and hail maximum. For ordinary storms, no significant increase is visible, even at the time of EchoMax. This suggests that with an increasing quantity of frozen hydrometeors in the updraught volume, the friction among supercooled and solid particles and therefore the transfer of charge from small to larger particles in the storms tends to increase. These results are in accordance with previous literature, where the storms' electrical activity was analysed and discussed in detail (e.g. Illingworth, 1985; Saunders, 1993). However, due to the large uncertainty and the limited time between the moment of lightning density and rate increases and the moment of hail initiation, it is questionable to use these parameters as precursors for hail and therefore for nowcasting purposes. These gradients have a slightly higher skill for the discrimination of potentially hail-bearing storms in areas where lightning data are available but not radar imagery. Considering satellite data with thunderstorm tracking algorithms and current (e.g. Goodman *et al.*, 2013) and future (e.g. Stuhlmann *et al.*, 2005) satellite-based lightning imagers or large extended ground-based lightning detection networks, it will be possible to obtain regional- or continental-scale hail climatologies based on these hail proxies. Punge *et al.* (2017) already used storm overshooting tops in combination with reanalysis data as proxies for hail hazard estimations, while Mroz *et al.* (2017), Ni *et al.* (2017) or Bang and Cecil (2019) rely on satellite passive microwave radiometers.

As expected, LJs provide some more skill for different lead times for hail nowcasting if compared with other lightning characteristics. The maximum in LJ detected around 20 min before hail initiation for all hailstorm categories is promising. However, LJs are detected even in the mature stage of the storms and not only in the initiation and intensification stage. The frequency of the LJs shows

a certain relation to the hailstorm intensity. If we consider the LJs only in the phases before hail initiation, it can be noticed that the frequency does not change for the different hailstorm classes. But if we consider LJs throughout the storm life cycle, their frequency becomes higher as the size of hailstones increases. However, the relation between LJs and storm microphysics is not really obvious, even though some hypotheses exist (Schultz *et al.*, 2017). It must be considered that storms producing large hailstones on average are longer lasting (Nisi *et al.*, 2018). The relative increase of LJs could also be explained by a longer life cycle.

Preliminary skill score quantifications obtained for nowcasting hail initiation with LJs are only partially encouraging. Despite a low FAR, the POD, and consequently the CSI, are low. Only when considering the entire life cycle of the storms in the statistics are increased skill scores obtained. However, in the latter case, LJs are then used more as discriminators between ordinary storms and hailstorms than as a precursor of hail. This potential for discrimination among storms' intensities, however, should not be underestimated. Several studies demonstrated that for storm nowcasting purposes both lightning rates and sigma-level amplitudes should be considered together. According to Chronis *et al.* (2015) and Schultz *et al.* (2015), both parameters must be analysed together in order to assess the storm intensity using lightning data; there is a large tendency that higher lightning rates and high sigma-level jumps produce stronger and longer-lasting storms. For this purpose, Wapler (2017) proposes an "LJs intensity matrix", which is a function of total lightning rate and LJ intensity (figure 12 in Wapler, 2017). If a sufficiently large dataset of ordinary and severe storms and homogeneous lightning data is available, such matrices may help in better discriminating the most severe storms taking into account the local climatological information about LJ occurrences and intensities as well as lightning detection network characteristics. Unfortunately, because of some homogeneity issues in the lightning data and the resulting smaller dataset, the computed matrices (not shown in this article) are statistically not representative and at the current stage cannot be used as a basis for nowcasting algorithms.

6 | SUMMARY AND CONCLUSIONS

In the present study, raster-based analyses of hail frequency (Nisi *et al.*, 2016) and an object-based approach to detect hailstorm initiation (Nisi *et al.*, 2018) are combined to investigate the diurnal cycle, spatio-temporal characteristics and lightning properties of convective storms. For this, more than 100,000 ordinary and 30,000

hail storms observed between 2002 and 2017 are considered. A multi-source analysis is performed including 4D radar data, lightning data, a cold-front climatology and a digital elevation model.

We find a distinct diurnal cycle in the median altitude of storm initiation locations. During daytime the average movement of the storms during intensification and mature stages is upslope, indicating that the Alpine pumping may play a major role. During night-time, the storms show an average opposite movement: thermal fronts and convergences due to katabatic wind systems and cold outflows supposedly are the main trigger and steer the storm during intensification stages.

The fact that large-scale cold fronts can only marginally explain the variability in extreme hail years underlines the importance of better understanding the regional-to-local patterns of hailstorm variability. Five years that all have an overall positive hail anomaly over the study area nevertheless show diverging distributions of the diurnal hail occurrence. Three out of the five years (2006, 2008 and 2017) show a typical diurnal cycle with hail maximum occurrence during the late afternoon. The other two years (2003 and 2009) show a more homogeneous diurnal behaviour with relative maxima occurring even during night-time (2003). When related to cold fronts over the region, it is demonstrated that the cold-front frequency alone only marginally explains the large differences between pronounced diurnal cycles in some extreme years versus night-time maxima in other years. Convection-relevant parameters like instability, low-level moisture availability and wind shear play important roles, but data are often less straightforward to interpret in complex and high Alpine terrain, since models and observations both come with considerable uncertainties in databases. Further study is needed to better understand how these regional circulation systems, which are distinct in the mountainous region of the Alps, affect the variability of hailstorm occurrence on different temporal and spatial scales.

The 4D radar characteristics of ordinary and hail storms are analysed by means of VIL and VILD time series. As expected, hailstorms show higher values compared to ordinary storms. However, a rapid increase of these values is only found shortly before hail initiation. Consequently, observations of VIL and VILD may be useful for discriminating ordinary from hailstorms but the use for nowcasting purposes is challenging. Thanks to a stronger dependence on the air-mass characteristics, VILD outperforms VIL in estimating the storm intensity, especially during cold air-mass conditions. Correlation scores between storms based on VIL and VILD show a seasonal cycle. Considering more than 130,000 storms, VIL-VILD correlations are low in April–September (0.56–0.6) and

high in July (0.81–0.89). The correlation is particularly low in cold air masses and low-topped storms.

Lightning analyses show a certain relation between lightning parameter changes and hail occurrence. However, the relation between lightning and storm microphysics is not obvious. Overall, hailstorms show a higher number of positive and negative CG and IC flashes than ordinary storms. The fraction of flash types taking into account the entire life cycle of storms shows no significant changes for all storm types. The large predominance of IC is present throughout the entire storm life cycles. The fraction of IC is between 60 and 79%, that of CG- between 12 and 38% and of CG+ between 2 and 11%. The peak current of ordinary storms is weaker (median: 0.1–2.5 kA) than that of hailstorms (median: 7–11 kA). Fifteen minutes prior to hail initiation a rapid increase of the peak current occurs. The increase of peak currents of CG- strikes starts earlier (40 min before hail initiation) and becomes abrupt in close proximity to hail initiation. For both CG+ and CG-, maximum peak current is reached 10–15 min after hail maximum.

The distinction between ordinary cells and hailstorms is evident if comparing time series of flash rates and densities. These two parameters show an increase in close proximity to hail initiations. These increases are visible considering all IC, CG- and TOTLI rates and densities. According to the literature, one of the most promising lightning parameters for nowcasting is represented by LJs. Considering LJs prior to hail initiation only, an average lead time of about 20 min is obtained. However, LJs are detected in the mature phase of the storms and in ordinary storms as well. LJs can be used as hail precursors with a POD of about 0.45 and an FAR of about 0.30. LJs show some more skills for the discrimination between ordinary and hail storms with a POD of 0.55 and an FAR of 0.3. Consequently even though LJs provide in some cases valuable information, the limited lead time and skill scores make the real-time application challenging.

In summary, the analysis showed that there is potential to derive meaningful information on hailstorm initiation and evolution from climatological datasets of radar-derived hail data and additional convection-relevant variables. At the Swiss national weather service MeteoSwiss, a first prototype working with the conventional low-frequency and very-low-frequency lightning detection network is running in real-time to detect LJs. Efforts are put into the discrimination between ordinary and hail storms based on combined thresholds on both sigma-level intensity and lightning rate.

Furthermore, efforts are underway to better understand patterns of hailstorm occurrence from a climatological perspective and machine learning algorithms will be used to predict storm motion,

intensifications and hail occurrence on the nowcasting time-scale.

ACKNOWLEDGMENTS

The authors thank all colleagues at MeteoSwiss for scientific discussion and suggestions. We would also kindly thank S. Schemm (ETH Zürich) for the cold-front climatology.

ORCID

L. Nisi  <https://orcid.org/0000-0003-4927-7660>

U. Germann  <https://orcid.org/0000-0002-8539-7080>

K. Schroeer  <https://orcid.org/0000-0002-2535-6658>

H. Barras  <https://orcid.org/0000-0002-1455-8895>

M. Kunz  <https://orcid.org/0000-0002-0202-9558>

O. Martius  <https://orcid.org/0000-0002-8645-4702>

REFERENCES

- Amburn, S.A. and Wolf, P.L. (1997) VIL density as a hail indicator. *Weather and Forecasting*, 12(3), 473–478.
- Azadifar, M., Rachidi, F., Rubinstein, M., Paolone, M., Diendorfer, G., Pichler, H., Schulz, W., Pavanello, D. and Romero, C. (2016) Evaluation of the performance characteristics of the European lightning detection network EUCLID in the Alps region for upward negative flashes using direct measurements at the instrumented Säntis tower. *Journal of Geophysical Research: Atmospheres*, 121(2), 595–606.
- Balakrishnan, N. and Zrnić, D.S. (1990) Estimation of rain and hail rates in mixed-phase precipitation. *Journal of the Atmospheric Sciences*, 47(5), 565–583.
- Bang, S.D. and Cecil, D.J. (2019) Constructing a multifrequency passive microwave hail retrieval and climatology in the GPM domain. *Journal of Applied Meteorology and Climatology*, 58(9), 1889–1904. <https://doi.org/10.1175/JAMC-D-19-0042.1>
- Biasutti, M., Yuter, S., Burleyson, C. and Sobel, A. (2011) Very high resolution rainfall patterns measured by TRMM precipitation radar: seasonal and diurnal cycles. *Climate Dynamics*, 39, 239–258.
- Bica, B., Knabl, T., Steinacker, R., Ratheiser, M., Dorninger, M., Lotteraner, C., Schneider, S., Chimani, B., Gepp, W. and Tschannett, S. (2007) Thermally and dynamically induced pressure features over complex terrain from high-resolution analyses. *Journal of Applied Meteorology and Climatology*, 46(1), 50–65.
- Billet, J., DeLisi, M., Smith, B.G. and Gates, C. (1997) Use of regression techniques to predict hail size and the probability of large hail. *Weather and Forecasting*, 12(1), 154–164. [https://doi.org/10.1175/1520-0434\(1997\)012<0154:UORTTP>2.0.CO;2](https://doi.org/10.1175/1520-0434(1997)012<0154:UORTTP>2.0.CO;2)
- Brooks, H.E. (2009) Proximity soundings for severe convection for Europe and the United States from reanalysis data. *Atmospheric Research*, 93, 546–553. <https://doi.org/10.1016/j.atmosres.2008.10.005>
- Carbone, R. and Tuttle, J. (2008) Rainfall occurrence in the US warm season: the diurnal cycle. *Journal of Climate*, 21, 4132–4146.
- Carey, L.D. and Rutledge, S.A. (1996) A multiparameter radar case study of the microphysical and kinematic evolution of a lightning producing storm. *Meteorology and Atmospheric Physics*, 59(1–2), 33–64.
- Chronis, T., Carey, L.D., Schultz, C.J., Schultz, E.V., Calhoun, K.M. and Goodman, S.J. (2015) Exploring lightning jump characteristics. *Weather and Forecasting*, 30(1), 23–37. <https://doi.org/10.1175/WAF-D-14-00064.1>
- Cintineo, J.L., Smith, T.M. and Lakshmanan, V. (2012) An objective high-resolution hail climatology of the contiguous United States. *Weather and Forecasting*, 27, 1235–1248.
- Darden, C.B., Nadler, D.J., Carcione, B.C., Blakeslee, R.J., Stano, G.T. and Buechler, D.E. (2010) Utilizing total lightning information to diagnose convective trends. *Bulletin of the American Meteorological Society*, 91(2), 167–176. <https://doi.org/10.1175/2009BAMS2808.1>
- Dee, D.P., Uppala, S.M., Simmons, A.J., Berrisford, P., Poli, P., Kobayashi, S., Andrae, U., Balmaseda, M.A., Balsamo, G., Bauer, P., Bechtold, P., Beljaars, A.C.M., van de Berg, L., Bidlot, J., Bormann, N., Delsol, C., Dragani, R., Fuentes, M., Geer, A.J., Haimberger, L., Healy, S.B., Hersbach, H., Hólm, E.V., Isaksen, I., Kållberg, P., Köhler, M., Matricardi, M., McNally, A.P., Monge-Sanz, B.M., Morcrette, J., Park, B., Peubey, C., de Rosnay, P., Tavolato, C., Thépaut, J.-N. and Vitart, F. (2011) The ERA-Interim reanalysis: configuration and performance of the data assimilation system. *Quarterly Journal of the Royal Meteorological Society*, 137(656), 553–597. <https://doi.org/10.1002/qj.828>
- Deierling, W. and Petersen, W.A. (2008) Total lightning activity as an indicator of updraft characteristics. *Journal of Geophysical Research*, 113, D16210. <https://doi.org/10.1029/2007JD009598>
- Dixon, M. and Wiener, G. (1993) TITAN: thunderstorm identification, tracking, analysis, and nowcasting – a radar-based methodology. *Journal of Atmospheric and Oceanic Technology*, 10, 785–797.
- Dotzek, N., Höller, H., Théry, C. and Fehr, T. (2001) Lightning evolution related to radar-derived microphysics in the 21 July 1998 EULINOX supercell storm. *Atmospheric Research*, 56(1–4), 335–354. [https://doi.org/10.1016/S0169-8095\(00\)00085-5](https://doi.org/10.1016/S0169-8095(00)00085-5)
- Edwards, R. and Thompson, R.L. (1998) Nationwide comparisons of hail size with WSR-88D vertically integrated liquid water and derived thermodynamic sounding data. *Weather and Forecasting*, 13, 277–285.
- Farnell, C., Rigo, T. and Pineda, N. (2017) Lightning jump as a nowcast predictor: application to severe weather events in Catalonia. *Atmospheric Research*, 183, 130–141. <https://doi.org/10.1016/j.atmosres.2016.08.021>
- Farnell, C., Rigo, T. and Pineda, N. (2018) Exploring radar and lightning variables associated with the lightning jump. Can we predict the size of hail? *Atmospheric Research*, 202, 175–186. <https://doi.org/10.1016/j.atmosres.2017.11.019>
- Faulkner, D.S. and Prudhomme, C. (1998) Mapping an index of extreme rainfall across the UK. *Hydrology and Earth System Sciences*, 2(2/3), 183–194.
- Fluck, E. (2017) *Hail potential over Western Europe*. PhD Thesis, Institute of Meteorology and Climate Research, Karlsruhe Institute of Technology (KIT), Karlsruhe, Germany, 142 pp.
- Foote, G.B. (1984) A study of hail growth utilizing observed storm conditions. *Journal of Applied Meteorology and Climatology*, 23(1), 84–101. [https://doi.org/10.1175/1520-0450\(1984\)023<0084:ASOHGU>2.0.CO;2](https://doi.org/10.1175/1520-0450(1984)023<0084:ASOHGU>2.0.CO;2)
- Foote, G.B., Krauss, T.W., and Makitov, V. (2005) Hail metrics using convective radar. In *Proceedings of 16th Conference on*

- Planned and Inadvertent Weather Modification, 10–13 January 2005, San Diego, CA.* Boston, MA: American Meteorological Society, pp 1–6.
- Foresti, L., Sideris, I.V., Panziera, L., Nerini, D. and Germann, U. (2018) A 10-year radar-based analysis of orographic precipitation growth and decay patterns over the Swiss Alpine region. *Quarterly Journal of the Royal Meteorological Society*, 144(716), 2277–2301. <https://doi.org/10.1002/qj.3364>.
- Gatlin, P.N. (2006) *Severe weather precursors in the lightning activity of Tennessee Valley thunderstorms.* Master thesis. The University of Alabama in Huntsville, AL.
- Gatlin, P.N. and Goodman, S.J. (2010) A total lightning trending algorithm to identify severe thunderstorms. *Journal of Atmospheric and Oceanic Technology*, 27(1), 3–22.
- Germann, U., Boscacci, M., Gabella, M. and Sartori, M. (2015) Radar design for prediction in the Swiss Alps. *Meteorological Technology International*, 4, 42–45.
- Germann, U., Boscacci, M., Gabella, M. and Schneebeli, M. (2016) Weather radar in Switzerland. In: Willemse, S. and Furger, M. (Eds.) *From weather observations to atmospheric and climate sciences in Switzerland.* Zurich, Switzerland: vdf Hochschulverlag AG ETH Zürich, pp. 165–188.
- Germann, U., Galli, G., Boscacci, M. and Bolliger, M. (2006) Radar precipitation measurement in a mountainous region. *Quarterly Journal of the Royal Meteorological Society*, 132(618), 1669–1692.
- Germann, U., Nerini, D., Sideris, I., Foresti, L., Hering, A. and Calpini, B. (2017) Real-time radar – a new Alpine radar network. *Meteorological Technology International*, 4, 88–92.
- Goodman, S.J., Blakeslee, R., Christian, H., Koshak, W., Bailey, J., Hall, J., McCaul, E., Buechler, D., Darden, C., Burks, J., Bradshaw, T. and Gatlin, P. (2005) The North Alabama lightning mapping array: recent severe storm observations and future prospects. *Atmospheric Research*, 76(1–4), 423–437. <https://doi.org/10.1016/j.atmosres.2004.11.035>.
- Goodman, S.J., Blakeslee, R.J., Koshak, W.J., Mach, D., Bailey, J., Buechler, D., Carey, L., Schultz, C., Bateman, M., McCaul, E., Jr. and Stano, G. (2013) The GOES-R geostationary lightning mapper (GLM). *Atmospheric Research*, 125, 34–49. <https://doi.org/10.1016/j.atmosres.2013.01.006>.
- Goudenhoofd, E. and Delobbe, L. (2013) Statistical characteristics of convective storms in Belgium derived from volumetric weather radar observations. *Journal of Applied Meteorology and Climatology*, 52(4), 918–934. <https://doi.org/10.1175/JAMC-D-12-079.1>.
- Greene, D., Robert, R. and Clark, A. (1972) Vertically integrated liquid water – a new analysis tool. *Monthly Weather Review*, 100, 548–552. [https://doi.org/10.1175/1520-0493\(1972\)100<0548:VILWNA>2.3.CO;2](https://doi.org/10.1175/1520-0493(1972)100<0548:VILWNA>2.3.CO;2).
- Hamann, U., Leonarduzzi, E., Clementi, L., Hering, A.M., Nisi, L., Sassi, M. and Germann, U. (2017) Nowcasting of thunderstorms and severe convection in Switzerland. *Oral presentation, 2nd European Nowcasting Conference 2017, Offenbach, Germany.*
- Handwerker, J. (2002) Cell tracking with TRACE3D – a new algorithm. *Atmospheric Research*, 61, 15–34. [https://doi.org/10.1016/S0169-8095\(01\)00100-4](https://doi.org/10.1016/S0169-8095(01)00100-4).
- Heinselman, P.L. and Ryzhkov, A.V. (2006) Validation of polarimetric hail detection. *Weather and Forecasting*, 21(5), 839–850. <https://doi.org/10.1175/WAF956.1>.
- Hengstebeck, T., Wapler, K., Heizenreder, D. and Joe, P. (2018) Radar network-based detection of mesocyclones at the German weather service. *Journal of Atmospheric and Oceanic Technology*, 35(2), 299–321. <https://doi.org/10.1175/JTECH-D-16-0230.1>.
- Hering, A.M., Germann, U., Boscacci, M. and Sényi, S. (2008) Operational nowcasting of thunderstorms in the Alps during MAP D-PHASE. In *Proceedings of 5th European Conference on Radar in Meteorology and Hydrology (ERAD), 30 June–4 July 2008, Helsinki, Finland.* Göttingen, Germany: Copernicus, pp 1–5.
- Hewson, D.T. (1998) Objective fronts. *Meteorological Applications*, 5, 37–65. <https://doi.org/10.1017/S1350482798000553>.
- Hirose, M., Oki, R., Shimizu, S., Kachi, M. and Higashiwa-toko, T. (2008) Finescale diurnal rainfall statistics refined from eight years of TRMM PR data. *Journal of Applied Meteorology and Climatology*, 47, 544–561. <https://doi.org/10.1175/2007JAMC1559.1>.
- Höller, H., Bringi, V.N., Hubbert, J., Hagen, M. and Meischner, P.F. (1994) Life cycle and precipitation formation in a hybrid-type hailstorm revealed by polarimetric and Doppler radar measurements. *Journal of the Atmospheric Sciences*, 51, 2500–2522. [https://doi.org/10.1175/1520-0469\(1994\)051<2500:LCAPFI>2.0.CO;2](https://doi.org/10.1175/1520-0469(1994)051<2500:LCAPFI>2.0.CO;2).
- Huuskonen, A., Saltikoff, E. and Holleman, I. (2014) The operational weather radar network in Europe. *Bulletin of the American Meteorological Society*, 95(6), 897–907. <https://doi.org/10.1175/BAMS-D-12-00216.1>.
- Illingworth, A.J. (1985) Charge separation in thunderstorms: small scale processes. *Journal of Geophysical Research*, 90(D4), 6026–6032. <https://doi.org/10.1029/JD090iD04p06026>.
- Jenker, J., Sprenger, M., Schwiertz, C., Dierer, S. and Leuenberger, D. (2010) Detection and climatology of fronts in a high-resolution model reanalysis over the Alps. *Meteorological Applications*, 17, 1–18. <https://doi.org/10.1002/met.142>.
- Joe, P., Burgess, D., Potts, R., Keenan, T., Stumpf, G. and Treloar, A. (2004) The S2K severe weather detection algorithms and their performance. *Weather and Forecasting*, 19, 43–63. [https://doi.org/10.1175/1520-0434\(2004\)019<0043:TSSWDA>2.0.CO;2](https://doi.org/10.1175/1520-0434(2004)019<0043:TSSWDA>2.0.CO;2).
- Johnson, J.T., MacKeen, P.L., Witt, A., Mitchell, E.D.W., Stumpf, G.J., Eilts, M.D. and Thomas, K.W. (1998) The storm cell identification and tracking algorithm: an enhanced WSR-88D algorithm. *Weather and Forecasting*, 13(2), 263–276. [https://doi.org/10.1175/1520-0434\(1998\)013<0263:TSCIAT>2.0.CO;2](https://doi.org/10.1175/1520-0434(1998)013<0263:TSCIAT>2.0.CO;2).
- Joss, J., Schaedler, B., Galli, G., Cavalli, R., Boscacci, M., Held, E., Della Bruna, G., Kappenberger, G., Nespor, V. and Spiess, R. (1998) *Operational use of radar for precipitation measurements in Switzerland.* Zürich, Switzerland: vdf Hochschulverlag AG ETH Zürich Available at: http://www.meteoswiss.admin.ch/content/dam/meteoswiss/fr/Mess-und-Prognosesysteme/doc/meteoswiss_operational_use_of_radar.pdf [Accessed 06 May 2019].
- Junghänel, T., Brendel, C., Winterrath, T. and Walter, A. (2016) Towards a radar- and observation-based hail climatology for Germany. *Meteorologische Zeitschrift*, 25(4), 435–445. <https://doi.org/10.1127/metz/2016/0734>.
- Kaltenböck, R., Diendorfer, G. and Dotzek, N. (2009) Evaluation of thunderstorm indices from ECMWF analyses, lightning data and severe storm reports. *Atmospheric Research*, 93(1–3), 381–396. <https://doi.org/10.1016/j.atmosres.2008.11.005>.
- Keil, C., Baur, F., Bachmann, K., Rasp, S., Schneider, L. and Barthlott, C. (2019) Relative contribution of soil moisture, boundary-layer and microphysical perturbations on convective predictability

- in different weather regimes. *Quarterly Journal of the Royal Meteorological Society*, 145(724), 3102–3115. <https://doi.org/10.1002/qj.3607>.
- Knapp, D.I. (1994) Using cloud-to-ground lightning data to identify tornadic thunderstorm signatures and nowcast severe weather. *National Weather Digest*, 19(2), 35–42.
- Kohn, M., Galanti, E., Price, C., Lagouvardos, K. and Kotroni, V. (2011) Nowcasting thunderstorms in the Mediterranean region using lightning data. *Atmospheric Research*, 100(4), 489–502. <https://doi.org/10.1016/j.atmosres.2010.08.010>.
- Kühnlein, C., Keil, C., Craig, G.C. and Gebhardt, C. (2014) The impact of downscaled initial condition perturbations on convective-scale ensemble forecasts of precipitation. *Quarterly Journal of the Royal Meteorological Society*, 140(682), 1552–1562. <https://doi.org/10.1002/qj.2238>.
- Kunz, M., Blahak, U., Handwerker, J., Schmidberger, M., Punge, H.J., Mohr, S., Fluck, E. and Bedka, K.M. (2018) The severe hailstorm in southwest Germany on 28 July 2013: characteristics, impacts and meteorological conditions. *Quarterly Journal of the Royal Meteorological Society*, 144(710), 231–250. <https://doi.org/10.1002/qj.3197>.
- Kunz, M. and Puskeiler, M. (2010) High-resolution assessment of the hail hazard over complex terrain from radar and insurance data. *Meteorologische Zeitschrift*, 19(5), 427–439. <https://doi.org/10.1127/0941-2948/2010/0452>.
- Lakshmanan, V. and Smith, T. (2009) Data mining storm attributes from spatial grids. *Journal of Atmospheric and Oceanic Technology*, 26(11), 2353–2365. <https://doi.org/10.1175/2009JTECHA1257.1>.
- Lang, T.J. and Rutledge, S.A. (2002) Relationships between convective storm kinematics, precipitation, and lightning. *Monthly Weather Review*, 130(10), 2492–2506. [https://doi.org/10.1175/1520-0493\(2002\)130<2492:RBCSKP>2.0.CO;2](https://doi.org/10.1175/1520-0493(2002)130<2492:RBCSKP>2.0.CO;2).
- Lombardo, K.A. and Colle, B.A. (2011) Convective storm structures and ambient conditions associated with severe weather over the northeast United States. *Weather and Forecasting*, 26(6), 940–956. <https://doi.org/10.1175/WAF-D-11-00002.1>.
- Lugauer, M. and Winkler, P. (2005) Thermal circulation in south Bavaria – climatology and synoptic aspects. *Meteorologische Zeitschrift*, 14(1), 15–30. <https://doi.org/10.1127/0941-2948/2005/0014-0015>.
- Lukach, M., Foresti, L., Giot, O. and Delobbe, L. (2017) Estimating the occurrence and severity of hail based on 10 years of observations from weather radar in Belgium. *Meteorological Applications*, 24(2), 250–259. <https://doi.org/10.1002/met.1623>.
- MacGorman, D.R., Burgess, D.W., Mazur, V., Rust, W.D., Taylor, W.L. and Johnson, B.C. (1989) Lightning rates relative to tornadic storm evolution on 22 May 1981. *Journal of the Atmospheric Sciences*, 46(2), 221–251. [https://doi.org/10.1175/1520-0469\(1989\)046<0221:LRRRTS>2.0.CO;2](https://doi.org/10.1175/1520-0469(1989)046<0221:LRRRTS>2.0.CO;2).
- Maddox, R.A., Zaras, D.S., MacKeen, P.L., Gourley, J.J., Rabin, R. and Howard, K.W. (1999) Echo height measurements with the WSR-88D: use of data from one versus two radars. *Weather and Forecasting*, 14(3), 455–460. [https://doi.org/10.1175/1520-0434\(1999\)014<0455:EHWMTW>2.0.CO;2](https://doi.org/10.1175/1520-0434(1999)014<0455:EHWMTW>2.0.CO;2).
- Mandapaka, P.V., Germann, U. and Panziera, L. (2013) Diurnal cycle of precipitation over complex Alpine orography: inferences from high-resolution radar observations. *Quarterly Journal of the Royal Meteorological Society*, 139(673), 1025–1046. <https://doi.org/10.1002/qj.2013>.
- Matsui, T., Mocko, D., Lee, M.-I., Tao, W.-K., Suarez, M.J. and Pielke Sr, R.A. (2010) Ten-year climatology of summertime diurnal rainfall rate over the conterminous US. *Geophysical Research Letters*, 37, L13807. <https://doi.org/10.1029/2010GL044139>.
- Mecikalski, J.R. and Bedka, K.M. (2006) Forecasting convective initiation by monitoring the evolution of moving cumulus in daytime GOES imagery. *Monthly Weather Review*, 134, 49–78.
- Miller, P.W., Ellis, A.W. and Keighton, S.J. (2015) The utility of total lightning trends in diagnosing single-cell thunderstorm severity: examples from the central Appalachians region. *Journal of Operational Meteorology*, 3(8), 82–98. <https://doi.org/10.15191/nwajom.2015.0308>.
- Mohr, S., Kunz, M. and Geyer, B. (2015) Hail potential in Europe based on a regional climate model hindcast. *Geophysical Research Letters*, 42, 10904–10912. <https://doi.org/10.1002/2015GL067118>.
- Mroz, K., Battaglia, A., Lang, T.J., Cecil, D.J., Tanelli, S. and Tridon, F. (2017) Hail-detection algorithm for the GPM Core Observatory satellite sensors. *Journal of Applied Meteorology and Climatology*, 56(7), 1939–1957. <https://doi.org/10.1175/JAMC-D-16-0368.1>.
- Nesbitt, S.W. and Zipser, E.J. (2003) The diurnal cycle of rainfall and convective intensity according to three years of TRMM measurements. *Journal of Climate*, 16(10), 1456–1475.
- Ni, X., Liu, C., Cecil, D.J. and Zhang, Q. (2017) On the detection of hail using satellite passive microwave radiometers and precipitation radar. *Journal of Applied Meteorology and Climatology*, 56(10), 2693–2709. <https://doi.org/10.1175/JAMC-D-17-0065.1>.
- Nisi, L., Ambrosetti, P. and Clementi, L. (2014) Nowcasting severe convection in the Alpine region: the COALITION approach. *Quarterly Journal of the Royal Meteorological Society*, 140(682), 1684–1699. <https://doi.org/10.1002/qj.2249>.
- Nisi, L., Hering, A., Germann, U. and Martius, O. (2018) A 15-year hail streak climatology for the Alpine region. *Quarterly Journal of the Royal Meteorological Society*, 144(714), 1429–1449. <https://doi.org/10.1002/qj.3286>.
- Nisi, L., Martius, O., Hering, A., Kunz, M. and Germann, U. (2016) Spatial and temporal distribution of hailstorms in the Alpine region: a long-term, high resolution, radar-based analysis. *Quarterly Journal of the Royal Meteorological Society*, 142(697), 1590–1604. <https://doi.org/10.1002/qj.2771>.
- Panziera, L., Gabella, M., Germann, U. and Martius, O. (2018) A 12-year radar-based climatology of daily and sub-daily extreme precipitation over the Swiss Alps. *International Journal of Climatology*, 38(10), 3749–3769. <https://doi.org/10.1002/joc.5528>.
- Panziera, L., Gabella, M., Zanini, S., Hering, A., Germann, U. and Berne, A. (2016) A radar-based regional extreme rainfall analysis to derive the thresholds for a novel automatic alert system in Switzerland. *Hydrology and Earth System Sciences*, 20(6), 2317–2332.
- Paxton, C.H. and Shepherd, J.M. (1993) *Radar diagnostic parameters as indicators of severe weather in central Florida*. NOAA Tech. Memo. NWS SR-149, 12 pp. Available from the National Weather Service Southern Region Headquarters, 819 Taylor Street, Room 10A26, Fort Worth, TX 76102.
- Piper, D. and Kunz, M. (2017) Spatio-temporal variability of lightning activity in Europe and the relation to the North Atlantic Oscillation teleconnection pattern. *Natural Hazards and Earth System Sciences*, 17, 1319–1336. <https://doi.org/10.5194/nhess-17-1319-2017>.

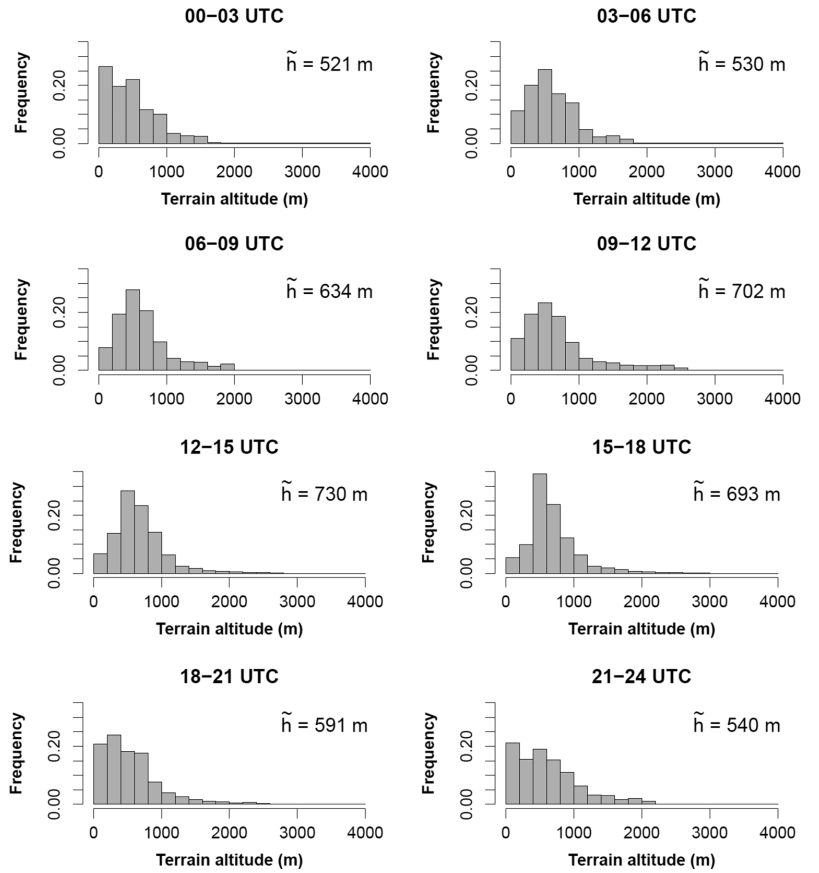
- Piper, D.A., Kunz, M., Allen, J.T. and Mohr, S. (2019) Investigation of the temporal variability of thunderstorms in Central and Western Europe and the relation to large-scale flow and teleconnection patterns. *Quarterly Journal of the Royal Meteorological Society*, 145(725), 3644–3666. <https://doi.org/10.1002/qj.3647>.
- Price, C. and Rind, D. (1993) What determines the cloud-to-ground lightning fraction in thunderstorms? *Geophysical Research Letters*, 20(6), 463–466.
- Punge, H.J., Bedka, K.M., Kunz, M. and Reinbold, A. (2017) Hail frequency estimation across Europe based on a combination of overshooting top detections and the ERA-Interim reanalysis. *Atmospheric Research*, 198, 34–43. <https://doi.org/10.1016/j.atmosres.2017.07.025>.
- Punge, H.J. and Kunz, M. (2016) Hail observations and hailstorm characteristics in Europe: a review. *Atmospheric Research*, 176–177, 159–184. <https://doi.org/10.1016/j.atmosres.2016.02.012>.
- Puskeiler, M., Kunz, M. and Schmidberger, M. (2016) Hail statistics for Germany derived from single-polarization radar data. *Atmospheric Research*, 178, 459–470. <https://doi.org/10.1016/j.atmosres.2016.04.014>.
- Rädler, A.T., Groenemeijer, P., Faust, E. and Sausen, R. (2018) Detecting severe weather trends using an additive regressive convective hazard model (AR-CHaMo). *Journal of Applied Meteorology and Climatology*, 57, 569–587. <https://doi.org/10.1175/JAMC-D-17-0132.1>.
- Roberts, R.D., Burgess, D. and Meister, M. (2006) Developing tools for nowcasting storm severity. *Weather and Forecasting*, 21, 540–558. <https://doi.org/10.1175/WAF930.1>.
- Roberts, R.D. and Rutledge, S. (2003) Nowcasting storm initiation and growth using GOES-8 and WSR-88D data. *Weather and Forecasting*, 18, 562–584.
- Rotach, M.W., Ambrosetti, P., Ament, F., Appenzeller, C., Arpagaus, M., Bauer, H.S., Behrendt, A., Bouttier, F., Buzzi, A., Corazza, M., Davolio, S., Denhard, M., Dorninger, M., Fontannaz, L., Frick, J., Fundel, F., Germann, U., Gorgas, T., Hegg, C., Hering, A., Keil, C., Liniger, M.A., Marsigli, C., McTaggart-Cowan, R., Montaini, A., Mylne, K., R.R., Richard, E., Rossa, A., Santos-Munoz, D., Schaer, C., Seity, Y., Staudinger, M., Stoll, M., Volkert, H., Walser, A., Wang, Y., Werhahn, J., Wulfmeier, W. and Zappa, M. (2009) MAP D-PHASE: real-time demonstration of weather forecast quality in the Alpine region. *Bulletin of the American Meteorological Society*, 90, 1321–1336.
- Ryzhkov, A.V., Kumjian, M.R., Ganson, S.M. and Khain, A.P. (2013) Polarimetric radar characteristics of melting hail. Part I: Theoretical simulations using spectral microphysical modeling. *Journal of Applied Meteorology and Climatology*, 52(12), 2849–2870. <https://doi.org/10.1175/JAMC-D-13-073.1>.
- Saunders, C.P.R. (1993) A review of thunderstorm electrification processes. *Journal of Applied Meteorology*, 32(4), 642–655. [https://doi.org/10.1175/1520-0450\(1993\)032<0642:AROTEP>2.0.CO;2](https://doi.org/10.1175/1520-0450(1993)032<0642:AROTEP>2.0.CO;2).
- Saxion, D.S. and Ice, R.L. (2012) New science for the WSR-88D: status of the dual-polarization upgrade. In *Proceedings of 28th Conference on Interactive Information Processing Systems, 22–26 January 2012, New Orleans, LA*. Boston, MA: American Meteorological Society. Available at: <https://ams.confex.com/ams/92Annual/webprogram/Paper197645.html> [Accessed 06 May 2019].
- Schemm, S., Nisi, L., Martinov, A., Leuenberger, D. and Martius, O. (2016) On the link between cold fronts and hail in Switzerland. *Atmospheric Science Letters*, 17, 315–325. <https://doi.org/10.1002/asl.660>.
- Schemm, S., Rudeva, I. and Simmonds, I. (2015) Extratropical fronts in the lower troposphere – global perspectives obtained from two automated methods. *Quarterly Journal of the Royal Meteorological Society*, 141(690), 1686–1698. <https://doi.org/10.1002/qj.2471>.
- Schemm, S. and Sprenger, M. (2015) Frontal-wave cyclogenesis in the North Atlantic – a climatological characterisation. *Quarterly Journal of the Royal Meteorological Society*, 141(693), 2989–3005. <https://doi.org/10.1002/qj.2584>.
- Schmidt, K., Hagen, M., Höller, H., Richard, E. and Volkert, H. (2012) Detailed flow, hydrometeor and lightning characteristics of an isolated thunderstorm during COPS. *Atmospheric Chemistry and Physics*, 12(15), 6679–6698.
- Schroerer, K. and Tye, M.R. (2019) Quantifying damage contributions from convective and stratiform weather types: how well do precipitation and discharge data indicate the risk? *Journal of Flood Risk Management*, 12, e12491. <https://doi.org/10.1111/jfr3.12491>.
- Schultz, C.J., Carey, L.D., Schultz, E.V. and Blakeslee, R.J. (2015) Insight into the kinematic and microphysical processes that control lightning jumps. *Weather and Forecasting*, 30(6), 1591–1621. <https://doi.org/10.1175/WAF-D-14-00147.1>.
- Schultz, C.J., Carey, L.D., Schultz, E.V. and Blakeslee, R.J. (2017) Kinematic and microphysical significance of lightning jumps versus nonjump increases in total flash rate. *Weather and Forecasting*, 32(1), 275–288. <https://doi.org/10.1175/WAF-D-15-0175.1>.
- Schultz, C.J., Petersen, W.A. and Carey, L.D. (2009) Preliminary development and evaluation of lightning jump algorithms for the real-time detection of severe weather. *Journal of Applied Meteorology and Climatology*, 48(12), 2543–2563. <https://doi.org/10.1175/2009JAMC2237.1>.
- Schultz, C.J., Petersen, W.A. and Carey, L.D. (2011) Lightning and severe weather: a comparison between total and cloud-to-ground lightning trends. *Weather and Forecasting*, 26(5), 744–755. <https://doi.org/10.1175/WAF-D-10-05026.1>.
- Schultz, E.V., Schultz, C.J., Carey, L.D., Cecil, D.J. and Bateman, M. (2016) Automated storm tracking and the lightning jump algorithm using GOES-R geostationary lightning mapper (GLM) proxy data. *Journal of Operational Meteorology*, 4(7), 92–107. <https://doi.org/10.15191/nwajom.2016.0407>.
- Schulz, W., Diendorfer, G., Pedebay, S. and Poelman, D.R. (2016) The European lightning location system EUCLID. Part 1: Performance analysis and validation. *Natural Hazards and Earth System Sciences*, 16(2), 595–605. <https://doi.org/10.5194/nhess-16-595-2016>.
- Shackford, C.R. (1960) Radar indications of a precipitation–lightning relationship in New England thunderstorms. *Journal of Meteorology*, 17(1), 15–19.
- Sideris, I.V., Gabella, M., Erdin, R. and Germann, U. (2014) Real-time radar–rain-gauge merging using spatio-temporal co-kriging with external drift in the alpine terrain of Switzerland. *Quarterly Journal of the Royal Meteorological Society*, 140(680), 1097–1111.
- Soderholm, J.S., McGowan, H., Richter, H., Walsh, K., Weckwerth, T.M. and Coleman, M. (2017) An 18-year climatology of hailstorm trends and related drivers across southeast Queensland, Australia. *Quarterly Journal of the Royal Meteorological Society*, 143(703), 1123–1135.
- Soriano, L.R. and De Pablo, F. (2007) Total flash density and the intracloud/cloud-to-ground lightning ratio over the Iberian

- Peninsula. *Journal of Geophysical Research*, 112, D13114. <https://doi.org/10.1029/2006JD007624>.
- Sprenger, M., Fragkoulidis, G., Binder, H., Croci-Maspoli, M., Graf, P., Grams, C.M., Knippertz, P., Madonna, E., Schemm, S., Škerlak, B. and Wernli, H. (2017) Global climatologies of Eulerian and Lagrangian flow features based on ERA-Interim. *Bulletin of the American Meteorological Society*, 98(8), 1739–1748.
- Stuhlmann, R., Rodriguez, A., Tjemkes, S., Grandell, J., Arriaga, A., Bézy, J.L., Aminou, D. and Bensi, P. (2005) Plans for EUMETSAT's third generation Meteosat geostationary satellite programme. *Advances in Space Research*, 36(5), 975–981. <https://doi.org/10.1016/j.asr.2005.03.091>.
- Surcel, M., Berenguer, M. and Zawadzki, I. (2010) The diurnal cycle of precipitation from continental radar mosaics and numerical weather prediction models. Part I: Methodology and seasonal comparison. *Monthly Weather Review*, 138, 3084–3106.
- Swisstopo. (2004) *DHM25 – the Digital Height Model of Switzerland*. Bern, Switzerland: Federal Office of Topography. Available at: <https://www.swisstopo.admin.ch/en/home/products/height/dhm25.html#ui-tab-788> [Accessed 06 May 2019].
- Trefalt, S., Martynov, A., Barras, H., Besic, N., Hering, A.M., Lenggenger, S., Noti, P., Röthlisberger, M., Schemm, S., Germann, U. and Martius, O. (2018) A severe hail storm in complex topography in Switzerland – observations and processes. *Atmospheric Research*, 209, 76–94. <https://doi.org/10.1016/j.atmosres.2018.03.007>.
- Treloar, A.B.A. (1996) Vertically integrated liquid water content as an indicator of severe hail in New South Wales. In *Preprints of 5th Australian Severe Thunderstorm Conference, 28 July–2 August 1996, Avoca Beach, New South Wales*. Melbourne: Australian Bureau of Meteorology, 48–51.
- Treloar, A.B.A. (1998) Vertically integrated radar reflectivity as an indicator of hail size in the Greater Sydney region of Australia. In *Proceedings of 19th Conference on Severe Local Storms, 14–18 September 1998, Minneapolis, MN*. Boston, MA: American Meteorological Society, 48–51.
- Twardosz, R. (2010) A synoptic analysis of the diurnal cycle of thunderstorm precipitation in Kraków (southern Poland). *International Journal of Climatology*, 30(7), 1008–1013. <https://doi.org/10.1002/joc.1960>.
- Uman, M.A. and Krider, E.P. (1982) A review of natural lightning: experimental data and modeling. *IEEE Transactions on Electromagnetic Compatibility*, 2, 79–112.
- Waldvogel, A., Federer, B. and Grimm, P. (1979) Criteria for the detection of hail cells. *Journal of Applied Meteorology*, 18, 1521–1525.
- Wallace, J.M. (1975) Diurnal variations in precipitation and thunderstorm frequency over the conterminous United States. *Monthly Weather Review*, 103(5), 406–419.
- Wapler, K. (2013) High-resolution climatology of lightning characteristics within Central Europe. *Meteorology and Atmospheric Physics*, 122(3–4), 175–184. <https://doi.org/10.1007/s00703-013-0285-1>.
- Wapler, K. (2017) The life-cycle of hailstorms: lightning, radar reflectivity and rotation characteristics. *Atmospheric Research*, 193, 60–72.
- Wapler, K., Goeber, M. and Trepte, S. (2012) Comparative verification of different nowcasting systems to support optimisation of thunderstorm warnings. *Advances in Science and Research*, 8(1), 121–127. <https://doi.org/10.5194/asr-1-1-2012>.
- Wapler, K., Harnisch, F., Pardowitz, T. and Senf, F. (2015) Characterisation and predictability of a strong and a weak forcing severe convective event – a multi-data approach. *Meteorologische Zeitschrift*, 24, 393–410. <https://doi.org/10.1127/metz/2015/0625>.
- Wapler, K., Hengstebeck, T. and Groenemeijer, P. (2016) Mesocyclones in Central Europe as seen by radar. *Atmospheric Research*, 168, 112–120.
- Warren, R.A., Ramsay, H.A., Siems, S.T., Manton, M.J., Peter, J.R., Protat, A. and Pillalamarri, A. (2020) Radar-based climatology of damaging hailstorms in Brisbane and Sydney, Australia. *Quarterly Journal of the Royal Meteorological Society*, 146(726), 505–530. <https://doi.org/10.1002/qj.3693>.
- Weissmann, M., Braun, F.J., Gantner, L., Mayr, G.J., Rahm, S. and Reitebuch, O. (2005) The Alpine mountain–plain circulation: airborne Doppler lidar measurements and numerical simulations. *Monthly Weather Review*, 133(11), 3095–3109.
- Wilks, D.S. (2006) *Statistical Methods in the Atmospheric Sciences: An introduction*, 2nd edition. Amsterdam, Netherlands: Academic Press.
- Williams, E., Boldi, B., Matlin, A., Weber, M., Hodanish, S., Sharp, D., Goodman, S., Raghavan, R. and Buechler, D. (1999) The behavior of total lightning activity in severe Florida thunderstorms. *Atmospheric Research*, 51(3–4), 245–265.
- Williams, E.R., Weber, M.E. and Orville, R.E. (1989) The relationship between lightning type and convective state of thunderclouds. *Journal of Geophysical Research*, 94(D11), 13213–13220.
- Witt, A., Eilts, M.D., Stumpf, G.J., Johnson, J.T., Mitchell, E.D. and Thomas, K.W. (1998) An enhanced hail detection algorithm for the WSR-88D. *Weather and Forecasting*, 13, 286–303.
- Yair, Y., Lynn, B., Price, C., Kotroni, V., Lagouvardos, K., Morin, E., Mugnai, A. and Llasat, M.D.C. (2010) Predicting the potential for lightning activity in Mediterranean storms based on the Weather Research and Forecasting (WRF) model dynamic and microphysical fields. *Journal of Geophysical Research*, 115, D04205. <https://doi.org/10.1029/2008JD010868>.
- Yuan, T., Remer, L.A., Pickering, K.E. and Yu, H. (2011) Observational evidence of aerosol enhancement of lightning activity and convective invigoration. *Geophysical Research Letters*, 38(4), L04701. <https://doi.org/10.1029/2010GL046052>.
- Zinner, T., Mannstein, H. and Tafferner, A. (2008) Cb-TRAM: tracking and monitoring severe convection from onset over rapid development to mature phase using multi-channel Meteosat-8 SEVIRI data. *Meteorology and Atmospheric Physics*, 101, 191–210.

How to cite this article: Nisi L, Hering A, Germann U, *et al.* Hailstorms in the Alpine region: Diurnal cycle, 4D-characteristics, and the nowcasting potential of lightning properties. *Q J R Meteorol Soc.* 2020;1–26. <https://doi.org/10.1002/qj.3897>

APPENDIX A.

FIGURE A1 Three-hourly distribution of altitudes of hailstorm initiation locations. \tilde{h} is the median altitude



APPENDIX B.

TABLE B1 Contingency table (Wilks, 2006) used to calculate LJs skill scores

		Observation (entire storm life cycle)		
		Hail	No hail	
Forecast	Before hail initiation for hailstorms or maxecho for ordinary storms)	LJ	2,506	1,070
		No LJ	3,011	35,673
Entire storm life cycle		LJ	3,013	1,266
		No LJ	2,504	34,602

APPENDIX C.

LIST OF ACRONYMS

COSMO: Consortium for Small-scale Modelling
COSMO-CH: COSMO Switzerland
COSMO-1: COSMO 1.0×1.0 km² resolution
COSMO-2: COSMO 2.2×2.2 km² resolution
COSMO-7: COSMO 6.6×6.6 km² resolution
CSI: Critical Success Index
DEM: Digital Elevation Model
DFRDT: “time rate of change of the total flash rate
within a thunderstorm”
ET15/ET45/ET50: 15 dBZ etc. Echo Top height
CG+: Positive Cloud to Ground lightning
CG-: Negative Cloud to Ground lightning
EUCLID: European Corporation for Lightning
Detection
FAR: False Alarm Rate
H0: Freezing Level Height
HII: Hailstorm Intensity Index
HST: Hailstreaks
HSW: Hailswath
IC: Intracloud lightning
LJ: Lightning Jump
MESH: Maximum Estimated Size of Hail
MESHS: Maximum Expected Severe Hail Size
NowPAL: Nowcasting of Precipitation AccumuLation
NWP: Numerical Weather Prediction
POD: Probability Of Detection
POH: Probability Of Hail
POSH: Probability of Severe Hail
SPA: Storm Path
STDEV: Standard Deviation
TFP: Thermal Front Parameter
TOTLI: Total Lightning
TRT: Thunderstorm Radar Tracking
UTC: Universal Time Coordinated
VIL: Vertically Integrated Liquid
VILD: Vertically Integrated Liquid Density